Journal of Marine Systems 142 (2015) 126–143

Contents lists available at ScienceDirect

Journal of Marine Systems

journal homepage: www.elsevier.com/locate/jmarsys

The North Atlantic subpolar circulation in an eddy-resolving global ocean model

Alice Marzocchi [a,*], Joël J.-M. Hirschi [b], N. Penny Holliday [b], Stuart A. Cunningham [b,1], Adam T. Blaker [b], Andrew C. Coward [b]

[a] School of Ocean and Earth Science, University of Southampton, National Oceanography Centre, European Way, Southampton SO14 3HZ, UK
[b] National Oceanography Centre, European Way, Southampton SO14 3ZH, UK

ARTICLE INFO

Article history:
Received 19 April 2013
Received in revised form 10 October 2014
Accepted 13 October 2014
Available online 30 October 2014

Keywords:
Ocean modelling
Eddy-resolving
NEMO
North Atlantic
Subpolar gyre warming
Physical oceanography

ABSTRACT

The subpolar North Atlantic represents a key region for global climate, but most numerical models still have well-described limitations in correctly simulating the local circulation patterns. Here, we present the analysis of a 30-year run with a global eddy-resolving (1/12°) version of the NEMO ocean model. Compared to the 1° and 1/4° equivalent versions, this simulation more realistically represents the shape of the Subpolar Gyre, the position of the North Atlantic Current, and the Gulf Stream separation. Other key improvements are found in the representation of boundary currents, multi-year variability of temperature and depth of winter mixing in the Labrador Sea, and the transport of overflows at the Greenland–Scotland Ridge. However, the salinity, stratification and mean depth of winter mixing in the Labrador Sea, and the density and depth of overflow water south of the sill, still present challenges to the model. This simulation also provides further insight into the spatio-temporal development of the warming event observed in the Subpolar Gyre in the mid 1990s, which appears to coincide with a phase of increased eddy activity in the southernmost part of the gyre. This may have provided a gateway through which heat would have propagated into the gyre's interior.

1. Introduction

The subpolar North Atlantic is one of the climatically relevant regions of the global ocean (Rhein et al., 2011). This is the first deep-ocean location where water mass transformation actively determines the shape of the Atlantic Meridional Overturning Circulation (AMOC). The subpolar North Atlantic is also a crucial region for the modulation of the temperate climate of north-western Europe, and the dynamics of the Subpolar Gyre (SPG) determine the rate of deep-water formation (Katsman et al., 2004). These newly formed, or significantly modified, water masses constitute the cold lower limb of the AMOC, and variations induced by climate change are most likely to arise in this area.

The SPG is a dominant large-scale feature of the surface circulation of the northwest Atlantic (Higginson et al., 2011) and is characterised by cyclonic rotation. It spans from 45°N to about 65°N (Rhein et al., 2011) and it includes the area of the sills between Greenland, Iceland, the Faroe Islands and Scotland. Waters of tropical and subtropical origin form the warm and salty upper branch of the AMOC; through the Gulf Stream, North Atlantic Current (NAC), and Irminger Current, the AMOC transports these warm and salty waters to the subpolar North Atlantic (Higginson et al., 2011; Käse and Krauss, 1996). Here, the NAC and the Irminger Current release heat to the atmosphere, and the subsequent buoyancy loss leads to the formation of deep and intermediate water throughout the subpolar gyre and notably in the Labrador Sea, from where it is exported as North Atlantic Deep Water (Rhein et al., 2011). The return cold and fresh stream flows along the shelf at the western edge of the basin. This comprises the East Greenland Current and the West Greenland Current, which carry sea-ice and low salinity water from the Arctic and runoff from North America and the Greenland ice cap (Dickson et al., 2007), providing a pathway for the export of fresh water from high latitudes (Higginson et al., 2011). The West Greenland Current flows into the Labrador Current, which exits the Labrador Sea on the western boundary and travels south past Newfoundland. The formation of deep and intermediate waters in the Labrador Sea is one of the major connections between the warm upper branch of the AMOC and its cold lower one, and a crucial process for the intensity of this link is the energy exchange between the atmosphere and the ocean surface (Rhein et al., 2011).

The dense, cold overflows from the Nordic Seas constitute the main source of the southward flow of North Atlantic Deep Water, maintaining the deep branch of the North Atlantic thermohaline circulation (Dickson and Brown, 1994; Eldevik et al., 2009; Hansen and Østerhus, 2000). The greatest volume exchange between the Nordic Seas and the rest of the world ocean occurs across the Greenland–Scotland ridge (Bacon, 2002), which separates these basins from the Atlantic Ocean. This

* Corresponding author at: School of Geographical Sciences, University of Bristol, University Road, Clifton, Bristol BS8 1SS, UK.
E-mail address: marzocchi.alice@gmail.com (A. Marzocchi).
[1] Now at: Scottish Association for Marine Science, Oban, UK.

http://dx.doi.org/10.1016/j.jmarsys.2014.10.007

ridge system between Greenland, Iceland, Faroe Islands and Scotland acts as a sill, damming up the deep-waters from the Nordic Seas, but allowing the exchange of surface and intermediate waters; some of these exchanges occur as overflows, when dense, cold waters from the Nordic Seas pass over the top of the sill and flow downstream at depth (Bacon, 2002). These processes have a fundamental impact on the circulation in the Labrador and Irminger Seas, which are active sites of deep-water formation. In these regions, wintertime cooling can trigger deep convection down to depths of 1000–2400 m, which results in the formation of an important intermediate water mass, the Labrador Sea Water (LSW). This watermass contributes to the lower limb of the global thermohaline circulation, which is a key process for the transport of heat, freshwater and carbon dioxide in the coupled atmosphere–ocean climate system (Haine et al., 2008; Yashayaev, 2007).

Modelling studies can be particularly useful given that most of the oceanic observational records in the subpolar North Atlantic are quite short and sparse. Estimates of the mean circulation based on such sampling may therefore be seasonally biased, significantly aliasing the low-frequency variability (Higginson et al., 2011). Numerical models represent therefore an invaluable tool to study the dynamics of these regions and to determine the causes of the observed variability, but they first need to be able to realistically simulate the base state of the regional circulation and hydrography (Rhein et al., 2011). Although many studies have shown that high-resolution eddy-permitting models can adequately reproduce the salient features of the circulation in the subpolar region (Tréguier et al., 2005) there are still questions with respect to hydrography and water masses formation (Rattan et al., 2010). For instance, numerical models tend to simulate an unrealistic salinification of the Labrador Sea, which can trigger too-deep convection, and cause an excessive deepening of the mixed layer in this area (Rattan et al., 2010; Treguier et al., 2005). The use of higher resolution, eddy-resolving models (i.e. able to resolve mesoscale eddies) could potentially overcome some of these biases, allowing a more realistic representation of the circulation.

The main limitations of running such high-resolution models are the computational and storage costs. However, state-of-the-art computing facilities allow the performance of relatively long runs with this kind of models, and therefore produce analysis of ocean processes at inter-annual to multi-decadal timescales. In this study we use a new version of the eddy-resolving ocean general circulation model (OGCM) NEMO (Nucleus for European Modelling of the Ocean) at a resolution of 1/12°, which is being run in its global configuration (ORCA12) by the Marine Systems Modelling group at the National Oceanography Centre, Southampton (NOCS), within the DRAKKAR Consortium (DRAKKAR Group, 2007). We investigate its performance in the North Atlantic subpolar regions, and present a 30-year (1978–2007) global simulation, which represents the longest available for this version of the model with a vertical resolution of 75 levels. The global ocean model configuration and the observational datasets are described in Section 2. In Section 3, we evaluate the representation of the circulation in the subpolar North Atlantic where key processes are analysed in specific areas of interest. Discussion, summary and conclusions are presented in Sections 4 and 5.

2. Methods and data

2.1. Ocean model configuration

The simulation analysed in this study was performed using a refined eddy-resolving OGCM at a resolution of 1/12°, which is part of the NEMO framework of Ocean/Sea-Ice general circulation models (Madec, 2008). NEMO is based on version 9.1 of the OPA primitive equation, free surface ocean general circulation model coupled to the Louvain la Neuve (LIM2) sea ice model (Fichefet and Maqueda, 1997), which is a dynamic–thermodynamic sea ice model with three layers and a viscous-plastic rheology (Renner et al., 2009). This simulation was started using version 3.2 of the model code, which was subsequently updated throughout the run (from model-year 1989 onwards) to version 3.3.1. NEMO uses the quasi-isotropic tripolar ORCA grid (Madec and Imbard, 1996), which becomes finer with increasing latitudes. In the case of ORCA12, the effective horizontal resolution of the common grid ranges between 9.25 km at the Equator, 7 km at Cape Hatteras (mid-latitudes), and 1.8 km in the Ross and Weddell Seas. The standard eddy-resolving ORCA12 configuration has been setup within the DRAKKAR group (e.g. Treguier et al., 2014; Duchez et al., 2014; Deshayes et al., 2013). This ORCA12 global configuration is run with some specific features at NOCS, such as a non-linear free surface to compute the sea surface height (SSH), DFS4.1 surface forcing (Brodeau et al., 2010), and 75 vertical levels. This vertical grid is refined at the surface (1 m for the first level), and has 22 levels in the first 100 m, smoothly increasing to a maximum layer thickness of 250 m at the bottom, with partial steps representing the bottom topography. The bathymetry used in ORCA12 is based on the combination of two databases, GEBCO (IOC, IHO and BODC, 2003) on the continental shelves, and ETOPO2 (U.S. Department of Commerce, 2006) in the open ocean. A free-slip lateral friction condition is applied at the lateral boundaries. A total variance diminishing advection scheme is used for the tracers (Cravatte et al., 2007; Lévy et al., 2001), and the mixing scheme is a turbulent closure model implemented by Blanke and Delecluse (1993).

The run was started from rest in 1978, and initialized from the World Ocean Atlas (WOA) 2005 climatological fields (Antonov et al., 2006; Locarnini et al., 2006). The ocean time step is 200 s and the sea ice model is called at every time step; the simulation is forced by 6-hourly winds, daily heat fluxes, and monthly precipitation fields, with a moderate relaxation of the surface salinity, which is restored to WOA 2005 with a 180-day timescale. The first three years of simulation were run without any constraint on the freshwater budget, but the resulting decrease in global SSH of 20 cm per year was considered unacceptable. This parameterization has therefore been modified, with the freshwater budget being instantly checked and restored when a deficit is found, but the restoring is only applied to areas where there is precipitation. An additional year (2008) has been run at the end of the initial simulation, to allow a more accurate comparison to available hydrographic measurements in the Labrador Sea (as outlined in Section 3.4.3, Fig. 11). This year was run using an updated version of the surface forcing (DFS5.1.1), and it is not included in the general analysis of the model's performance, which only considers the first 30 years of simulation. Model outputs are stored as successive 5-day means throughout the whole integration, and in this study we only consider the North Atlantic region, extracted from the global model output, with a domain spanning from about 90°W to 10°E, and 25°N to 75°N (Fig. 1).

2.2. Volume transport calculation

Full depth volume transport is calculated across five sections covering the main open boundaries of the analysed North Atlantic domain (Fig. 1b). Volume transport time series were produced for the whole duration of the simulation.

The volume transport of the overflows from the Nordic Seas is calculated in temperature classes, both in the Denmark Strait and in the Faroe Bank Channel, where two specific sections have been selected across the two channels, allowing comparison to observations. Temperature classes have been defined as described in Section 3.2, and a mask has been applied to select only the areas characterised by the selected temperature ranges. The volume transport is calculated as the velocity field (its meridional component in the Denmark Strait, and its zonal component in the Faroe Bank Channel) multiplied by

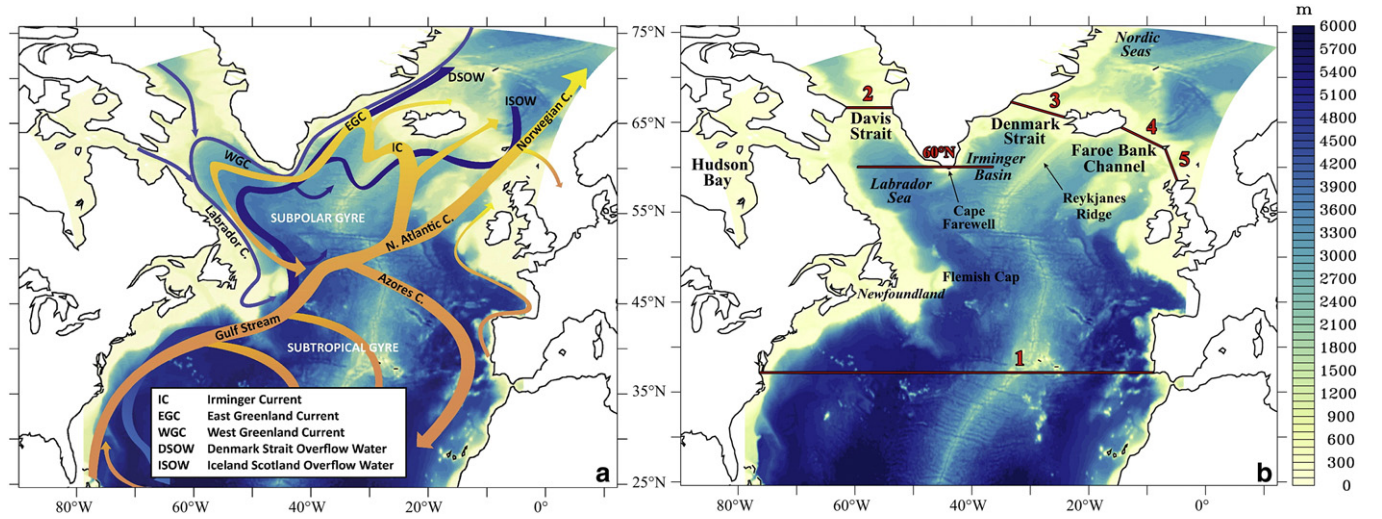

Fig. 1. Model's North Atlantic domain analysed in this study. (a) Main circulation patterns in this area. Deeper currents are in blue, shallower ones in orange/yellow. (b) Shaded is the bathymetry of the region. Red numbered lines indicate the five sections where the volume transport has been calculated. Number 1 represents a basin-wide section at 37°N, 2 is Davis Strait, 3 Denmark Strait, 4 crosses the Iceland-Faroe Ridge, and 5 spans between Faroe Islands and Scotland. The additional red line indicates the position of the section taken across the Labrador Sea and part of the Irminger Sea (60°N).

the grid area, and vertically integrated over the selected surface (determined by the aforementioned mask).

2.3. Observational datasets

Modelled sea surface temperature (SST) and sea surface salinity (SSS) fields are compared to the UK Met Office Hadley Centre observational dataset ENSEMBLES version 2a (EN3), an update of EN2 (Ingleby and Huddleston, 2007). The EN3 product consists of gridded mean fields for each month, derived from quality-controlled profiles of temperature and salinity, which are output in a model-independent monthly objective analysis. EN3 has a coarser horizontal resolution (1.25°) than the model, only 40 vertical levels, and the top layer is 10 m whereas in ORCA12 it is 1 m, but we have verified that this does not bias the comparison (not shown). This dataset represents a good basis for comparison, providing observations for an overlapping time frame which allowed us to compute the same climatologies between 1983 and 2007 both for the model output and the EN3 observational data. Modelled SST fields are also compared to the observed ones from the NOAA Optimum Interpolation (OI) SST V2 monthly time series (Reynolds and Smith, 1994; Reynolds et al., 2002).

To assess the realism of large scale surface current patterns we compare model output with absolute geostrophic velocities derived from satellite altimetry. The altimeter products were produced by Ssalto/Duacs and distributed by Aviso, with support from Cnes (http://www.aviso.oceanobs.com/duacs).

In the Labrador and Irminger Seas subsurface velocities are compared to observational data collected in August–September 2008 onboard the UK cruise Discovery 332 (Bacon, 2010). The data from this cruise are used because it was the first time that the Labrador Sea and Irminger Sea sections had been measured synoptically and with direct current measurements. Velocities normal to the hydrographic sections across the Labrador and Irminger Seas were derived as defined in Holliday et al. (2009). The locations of the hydrographic sections across the Labrador and Irminger Seas can be found in Bacon (2010) and Fig. 1b shows where the section was taken in the model.

The modelled volume transport for the overflows from the Nordic Seas is compared to two sets of continuous observational datasets. An updated mooring time series for the Denmark Strait Overflow is provided by Jochumsen et al. (2012), with measurements collected between October 2007 and July 2010, integrating and confirming the results obtained by Macrander et al. (2005) between 1999 and 2003, through the combination of in situ and modelled data. Measurements for the Faroe Bank Channel Overflow consist of data collected between 1995 and 2005 using a combination of ADCP and CTD measurements (Hansen and Østerhus, 2007), integrated with new estimates obtained between 2005 and 2010, providing an updated mean value for this time series (Bogi Hansen, personal communication).

3. Results

3.1. Model validation in the North Atlantic

The first step of the validation of ORCA12 in the subpolar North Atlantic consists of a comparison of surface variables from the numerical model output with observations, and an analysis of the overall structure of the circulation, to assess whether the main currents are resolved by the model and follow realistic pathways. This analysis is performed over a wider domain, comprising both the SPG and part of the Subtropical Gyre, to also monitor the Gulf Stream pathway and its separation, and the spread of waters of subpolar origin towards lower latitudes. Subsequently, local key features will be further investigated in specific regions of interest, such as the overflows from the Nordic Seas in the Denmark Strait and in the Faroe Bank Channel, and the mixed layer depth (MLD) and the Deep Western Boundary Current (DWBC) in the Labrador Sea. The main bathymetric features of the analysed North Atlantic domain are realistically represented in the model, such as the shape of the Mid-Atlantic Ridge, Reykjanes Ridge south of Iceland, and the Charlie-Gibbs fracture zone (Fig. 1).

During the initial phase of the run (spin-up), the model is subject to an initial drift due to the adjustment of the simulation from the initial WOA conditions towards the new state imposed by the surface forcing. There will also be an element of drift due to parameter choices, and a further element which arises from structural biases in the model where due to limitations such as the grid resolution or parameterisations the model is not able to correctly represent the dynamics of the real ocean. Strong initial drifts can persist for several years of simulation (Rattan et al., 2010), and weaker ones can affect a run for centuries, particularly in the deep ocean. ORCA12 is initialised with the WOA 2005 climatology, which has a much coarser resolution (1°) than the model and does not include fine scale details like the narrow boundary currents on the shelf regions and more generally close to continental boundaries. Nevertheless, after the initial adjustment phase, modelled surface properties such as SST and SSS can be tested against

observations. To assess the state of the simulation after 30 years of run, we compute climatologies of the months of January and July for the last 25 years of the run, and compare them with the corresponding data from the EN3 dataset (Figs. 2 and 3).

SST fields show the spread of warmer surface waters from the Atlantic into the subpolar regions (Fig. 2) and colder temperatures (below −1 °C in January) in areas that are mostly or partially ice covered, such as Hudson Strait, north of Davis Strait and north of Iceland. Modelled and observed values generally exhibit a matching distribution, especially in January, apart from the Labrador Sea, which is characterised by higher values in the model (up to 2 °C warmer in the northernmost part) than in the observations. In addition, the warm subtropical front (temperatures above 22 °C) is expanding further north in the observations, showing colder modelled SST values (up to 5 °C difference) between 30 and 40°N, especially in July. This could mean that the model does not stratify enough during the summer months, mixing down heat too easily. Hudson Strait and part of Hudson Bay also generally exhibit warmer temperatures in the observations than in the model, both in January and July.

The exchange of Atlantic waters with the Nordic Seas across the Greenland–Scotland Ridge can also be seen in the SSS maps (Fig. 3), and the pathway of the East Greenland Current flowing towards the Labrador Sea is also clearly visible. SSS values in the model generally show a good agreement with the EN3 observational dataset; however, the areas of the Labrador and Irminger Seas exhibit higher salinities in the model, both in January and July, with differences up to 1 g kg^{-1} in the northern part of the Labrador basin. It is important to note that for both SST and SSS fields some of the discrepancies are due to the higher resolution of the numerical model, which is able to resolve smaller scale features

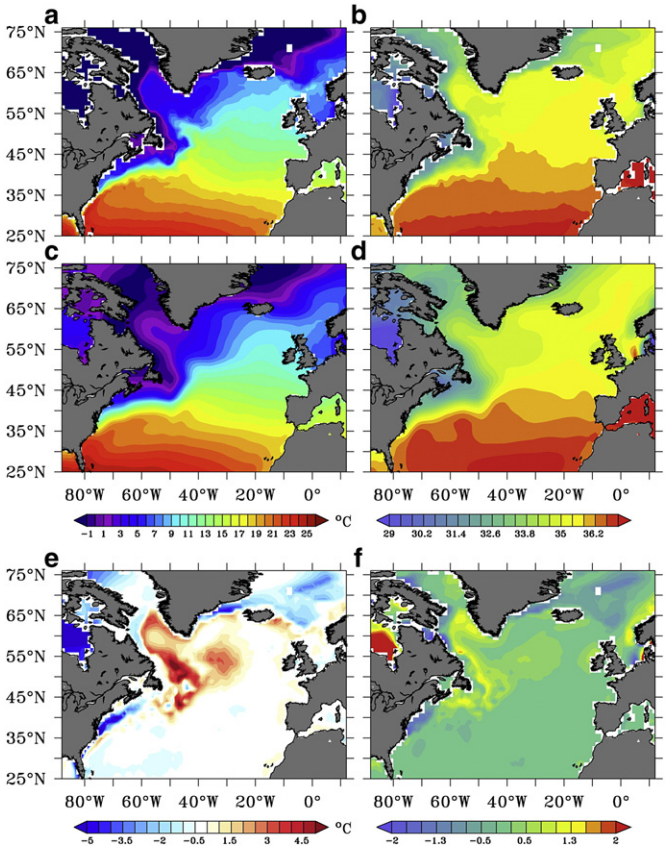

Fig. 2. Panels on the left (a, c, e) represent sea surface temperature values, and those on the right sea surface salinities (b, d, f) for the month of January, from a climatology of the last 25 years of the analysed run (1983–2007). Top panels portray ORCA12 output (a, b), mid panels the EN3 observational dataset (c, d), and bottom panels are the difference between ORCA12 output and the EN3 dataset (e, f).

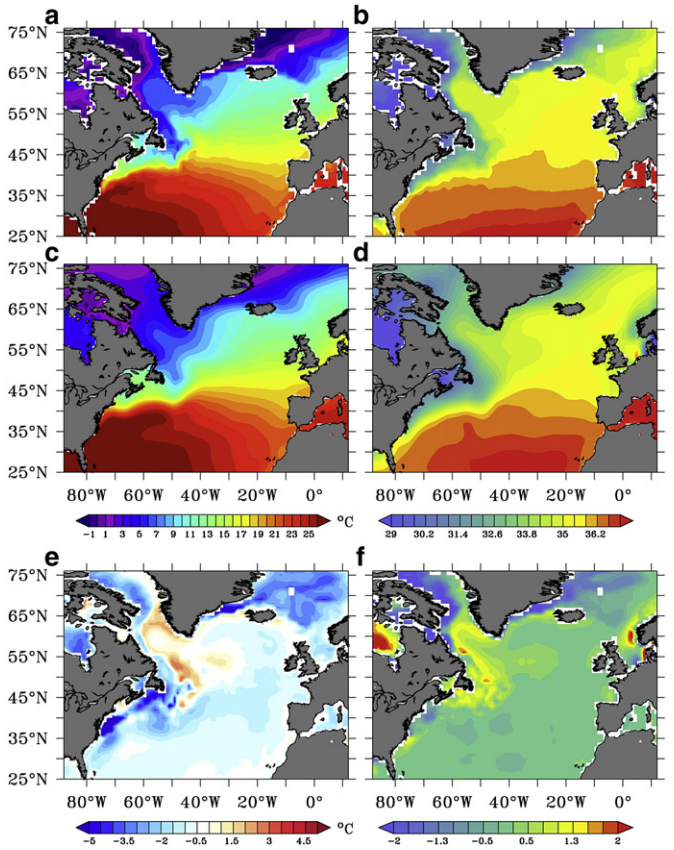

Fig. 3. Panels on the left (a, c, e) represent sea surface temperature values, those on the right sea surface salinities (b, d, f) for the month of July, from a climatology of the last 25 years of the analysed run (1983–2007). Top panels portray ORCA12 output (a, b), mid panels the EN3 observational dataset (c, d), and bottom panels are the difference between ORCA12 output and the EN3 dataset (e, f).

and currents (i.e. boundary currents or the tight fronts of the Gulf Stream) that are not present in the EN3 dataset. In addition, some biases in the observational dataset are due to a lack of measurements on the shelf and shallow areas in the north-western part of the domain (Grist et al., 2011).

SST fields in ORCA12 for the last year of the run (2007) have also been compared to the Reynolds SST dataset (Reynolds and Smith, 1994; Reynolds et al., 2002). To better assess the impact of model resolution we also consider ORCA1 and ORCA025 which are lower resolution (1° and 1/4°, respectively) versions of ORCA12 (Fig. 4a,b). Both ORCA1 and ORCA025 are run for the same time period (1978 to 2007) using the same surface forcing as ORCA12 (DFS 4.1). In the lower resolution runs the most striking difference is a cold bias compared to observations off Newfoundland, around Flemish Cap, and the Northwest Corner (between 47 and 52°N). This is most pronounced in ORCA1, with much colder temperatures (5°C or more) over that region and with the cold anomaly extending eastward to 20°W. This cold bias is also present in ORCA025, but is less severe and more spatially confined (eastward extent only to about 25°W). The warm bias found east of Iceland in ORCA1 disappears in ORCA025 where it is replaced by slightly colder than observed temperatures. All simulations show a similar bias towards colder modelled temperatures in the regions north of Iceland (up to 7.5 °C colder). Both ORCA1 and ORCA025 exhibit a warm bias along the US coast between 35 and 45°N, whereas in ORCA12 the cold and warm SST biases off Newfoundland and along the US coast largely disappear (Fig. 4c). The main remaining differences between ORCA12 and the observational dataset are confined to the boundary regions (e.g. along the US coast north of Cape Hatteras). However, rather than being a model bias, this could also reflect the model's ability to simulate fine scale features of the circulation (such as boundary currents and sharp SST fronts) that are absent from the Reynolds dataset.

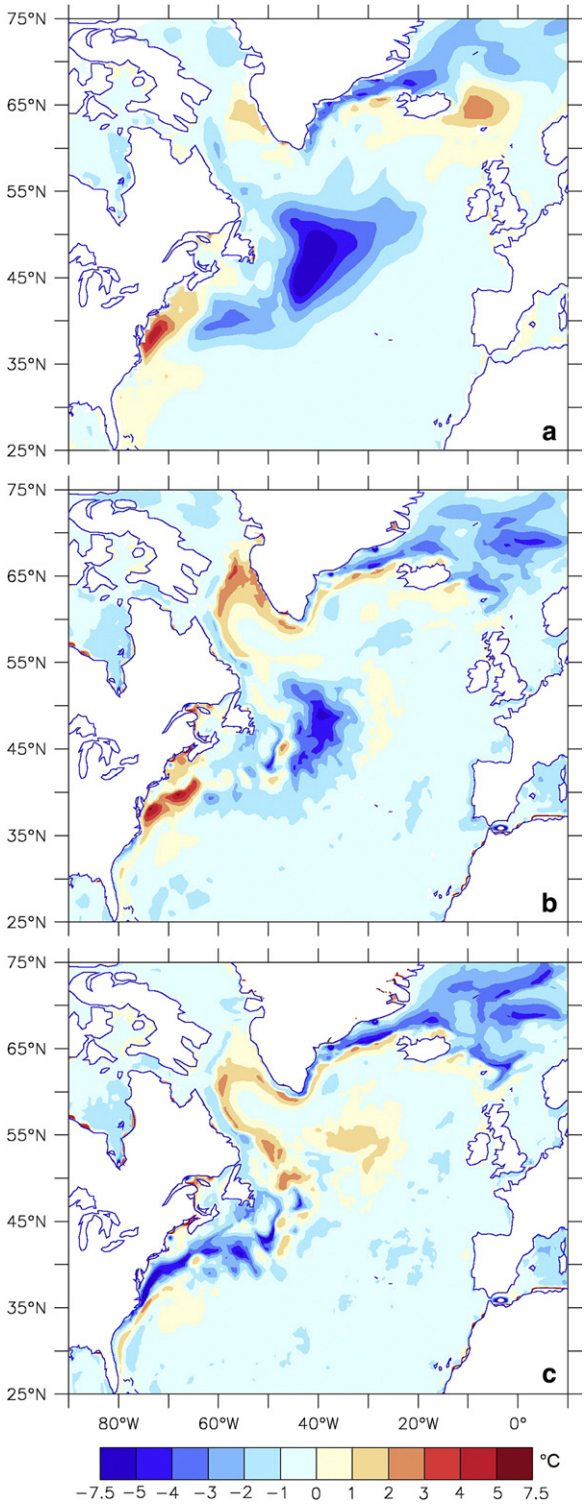

Fig. 4. Differences between modelled SSTs and the Reynolds observational dataset in 2007 (annual mean). The convention is model minus observations. a) ORCA1, b) ORCA025, c) ORCA12.

To further analyse the performance of the model in the North Atlantic we have taken five sections at the boundaries of this region (Fig. 1b) and calculated the full-depth volume transport across each section to obtain a volume budget for the analysed domain. The net transports through the English Channel and the Hudson Strait are not taken into account due to their minor contribution of ~0.1 Sv (Prandle et al., 1996; Straneo and Saucier, 2008), and also because they compensate each other (outflow and inflow, respectively). Transport time series have been produced for the whole duration of the run (Fig. 5) and mean values for the 30 years of run have been calculated for each section (Table 1). No clear trend or substantial variations can be identified in the time series, apart from the transport across Davis Strait, which stabilises only in the last 10 years of the run, but still shows an increasing trend. The transports through the Davis Strait, Iceland–Scotland Ridge, Denmark Strait, and 37°N largely balance. The net southward transport at 37°N reflects a Bering Strait transport of ~1.3 Sv, as well as a gain of freshwater over the Arctic Ocean. An overestimation of the transport at Bering Strait is also found in NEMO 1/4°, where the model inflow is 42% higher than that of the observations (Popova et al., 2010), suggesting values of ~0.8–0.9 Sv (Roach et al., 1995; Woodgate et al., 2005).

3.2. Overflows from the Nordic Seas

At the Greenland–Scotland Ridge it is also important to determine the strength of the transport occurring as overflows in the deepest parts of the sills. The two main cores of cold, dense waters from the Nordic Seas flow through the two deepest passages across the Greenland–Scotland Ridge, the Denmark Strait and the Faroe Bank Channel (Quadfasel and Käse, 2007); there is also a shallow overflow between Iceland and the Faroe Islands, but it has a relatively weak outlet (Hansen and Østerhus, 2000). The even weaker overflow across the Wyville–Thompson Ridge is not assessed in this study.

To assess whether the model is capable of simulating these key processes, surface (not shown) and bottom current velocities (Fig. 6) have been analysed both in the Denmark Strait and in the Faroe Bank Channel. Model results exhibit the presence of a barotropic flow passing through the sill in the Denmark Strait, as found in previous studies that described the barotropic structure of the current in this area, and found little shear (therefore little turbulence) between the overflow plume and the water masses above (Voet and Quadfasel, 2010). In the Faroe Bank Channel the flow does not show the same highly barotropic structure, with surface velocities dominated by the Atlantic inflow reaching the Nordic Seas. In the Denmark Strait a vigorous current with velocities reaching 0.6 m s^{-1} can also be seen at the bottom, and in the Faroe Bank Channel there is still a weaker stream passing through the sill, despite the intricate bathymetry of the area; in both cases the flow at the bottom realistically follows the bathymetric constraints of the sills (Fig. 6).

To estimate the strength of the overflows, the corresponding volume transport has been calculated both in the Denmark Strait and in the Faroe Bank Channel, across specific sections (as indicated in Fig. 6), using temperature classes (Fig. 7). The calculation of the transports depends on the determination of what part of the water column is constituted by waters of Arctic origins and is flowing as overflows. Here, the selected isotherms (5.5 °C in the Denmark Strait, and 7 °C in the Faroe Bank Channel) represent the fronts between the cold overflows and the warm Atlantic waters in the model (Fig. 7a, b), and correspond to the blue lines in the time series (Fig. 7c, d). To calculate the overflow transport we use these isotherms rather than those of isopycnals suggested by Voet and Quadfasel (2010) and Saunders (1990), because a bias in the simulated properties means that the data-derived definitions capture less than half of the model overflow water.

The mean transport calculated in model temperature classes for 30 years of simulation has been compared to in situ measurements from similar sections. The volume transport through Denmark Strait shows little variation, with only a slightly weakening trend (in terms of absolute value of the transport) in the first 10 years of simulation. The mean transport is 3.2 Sv, which favourably matches observed values (Jochumsen et al., 2012; Macrander et al., 2005). There is no clear seasonal cycle, as observed in other studies on the exchanges across the Greenland–Scotland Ridge, which also report a small seasonal variability of 1 Sv at the most (e.g. Hansen and Østerhus, 2007). In the Faroe

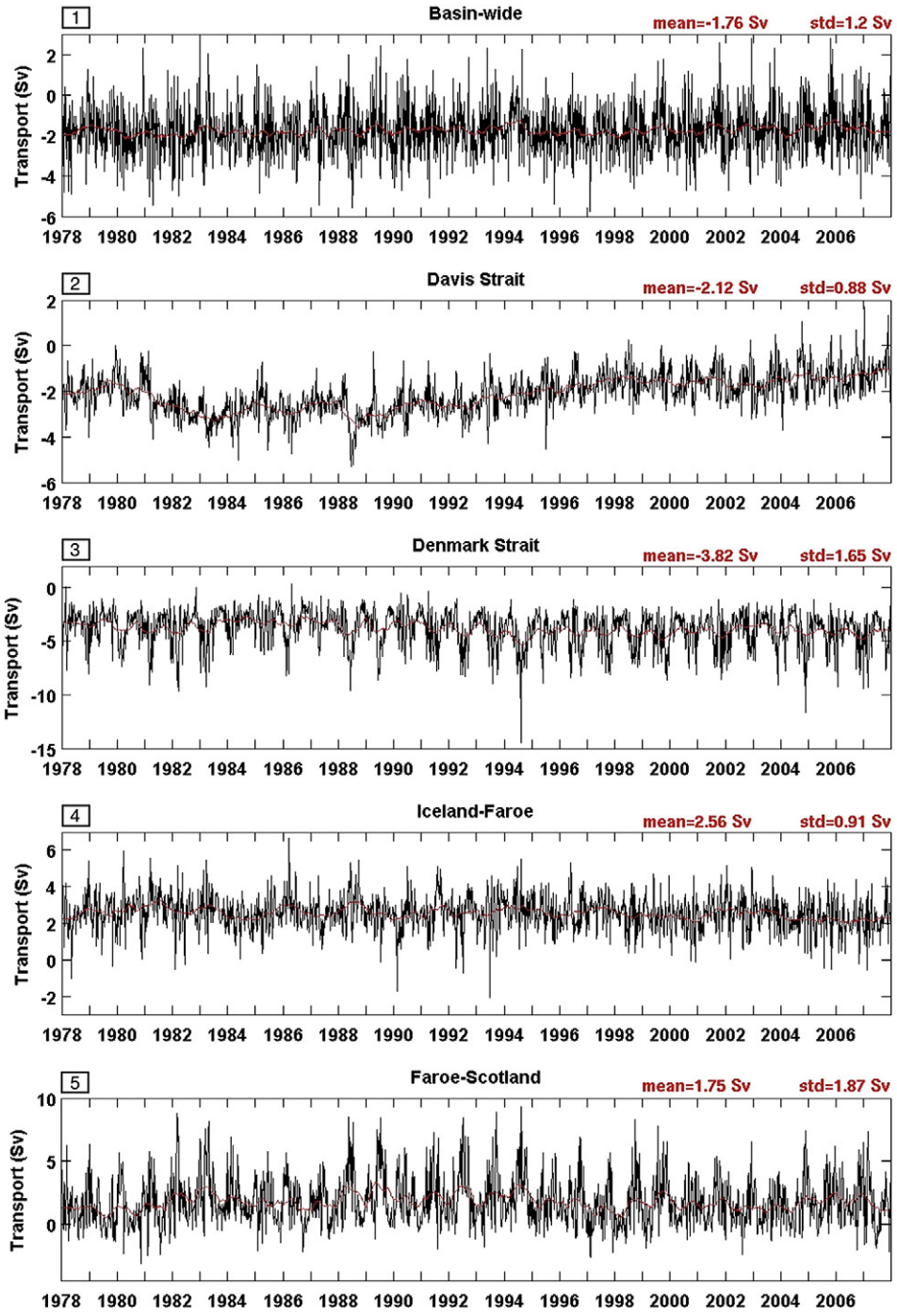

Fig. 5. Time series of volume transport calculated through the whole water column across the five sections indicated in Fig. 1 (see corresponding numbers, 1–5). Here the sign indicates the real direction of the flow, where positive values represent northward transport, and negative ones correspond to a southward flow.

Table 1
Volume transport budget for the North Atlantic. Volume transport is calculated through the whole water column across the five sections at the boundaries of the analysed North Atlantic domain (indicated in Fig. 1), and a mean value is taken for each section. Here the sign of the transport indicates whether the direction of the flow is into (+) the domain or out (−) of it.

Basin-wide at 37°N	−1.76 Sv
Davis Strait	2.12 Sv
Denmark Strait	3.82 Sv
Iceland–Faroe	−2.56 Sv
Iceland–Scotland	−1.75 Sv

Bank Channel the volume transport is weaker, with a mean value of 1.5 Sv, which is lower than the observed values of 2–2.1 Sv (Hansen and Østerhus, 2007; Bogi Hansen, personal communication). Also in this case, there is neither a clear seasonal cycle nor an evident trend, apart from a slight weakening until 1984, and the volume transport appears to be as steady as the one described by Hansen and Østerhus (2007), but ~0.5 Sv weaker. When calculated using the observed temperature classes (Fig. 7c, d; red lines), the mean values are 0.02 Sv for the Denmark Strait overflow and 0.2 Sv for the Faroe Bank Channel, since only a small part of the overflow is actually picked up using these temperature ranges. The abrupt oscillations between zero and some slightly higher values shown by the red lines in both time series

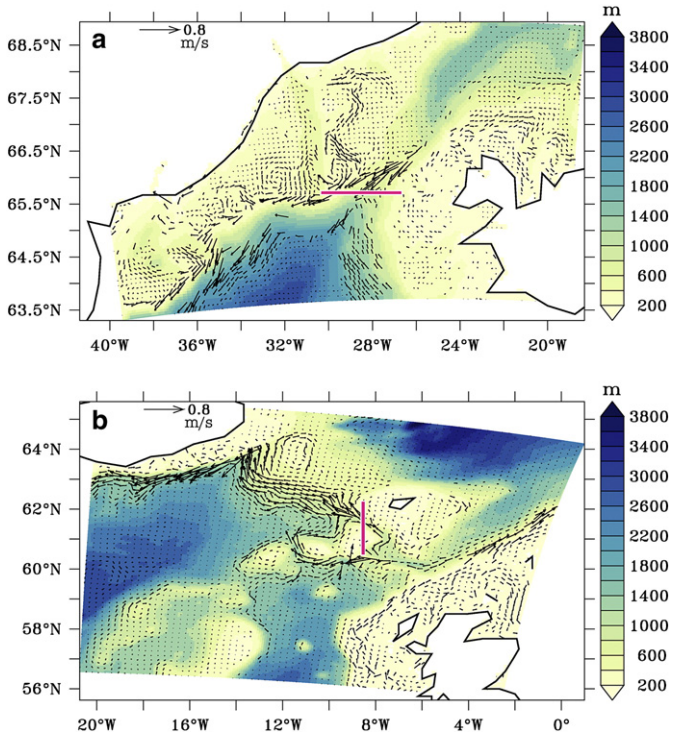

Fig. 6. Areas of the overflows from the Nordic Seas: Denmark Strait (a) and Faroe Bank Channel (b). Shaded is the bathymetry, and arrows represent bottom current velocities. The reference arrow size is 0.8 m s^{-1} and every second arrow is plotted. Magenta lines indicate the sections chosen for the calculation of the overflow volume transport shown in Fig. 7.

arise from an artefact created by the temperature classes used to define the water mass and the small number of model grid boxes concerned. The model does not create enough cold water, so there are times during which there is no water colder than 2.5–3 °C passing through the straits. However, the velocities associated with the overflow transports never vanish and are always southward (Denmark Strait) or westward (FBC). This means that at the times when the temperature still manages to fall below the threshold values (2.5–3 °C) the overflow transports will jump to a non-zero value set by the pre-existing velocity field, which gives the transports the artificial look seen in Fig. 7d (red line).

3.3. The subpolar circulation in ORCA12

ORCA12 shows a significant improvement in the pathways of North Atlantic currents compared to ORCA025 (Fig. 8e,f) even if at first sight the changes seen in ORCA12 appear less striking than when moving from ORCA1 (non eddying, Fig. 8a,b) to ORCA025 (eddy-permitting, Fig. 8c,d). Features such as eddies and sharp boundary currents are present in both ORCA025 and ORCA12. However, much more mesoscale activity can be seen in ORCA12 with ocean eddies being simulated not only in the vicinity of the Gulf Stream and its extension (Fig. 8d) but also in the basin interior, including the centre of the gyres (Fig. 8f). Increasing the model's resolution leads to an overall increase of the absolute velocities (up to 0.5 m s^{-1}, or more), not only for western boundary currents but also for the entire domain, as shown by the comparison of average surface velocities for year 2007 in ORCA1, ORCA025, and ORCA12 (Fig. 8a–f). In ORCA025 the average velocities are weaker than those inferred from satellite altimetry (Fig. 8c,g). The comparison with satellite-based geostrophic velocities also illustrates the significant improvements in the representation of current pathways in ORCA12 (Fig. 8e–h). In ORCA12 the separation of the Gulf Stream from the US coast occurs at Cape Hatteras at 35°N, as seen in the satellite data. In ORCA025 the Gulf Stream overshoots Cape Hatteras and separates too far north (Fig. 8c,d). We note that the Gulf Stream also overshoots at the beginning of the ORCA12 simulation, and it is only after about 1–1.5 years that the separation point moves south of Cape Hatteras where it then remains for the rest of the simulation (not shown). The Azores Current realistically develops from the Gulf Stream at 36°N and reaches the Straits of Gibraltar exhibiting maximum velocities of 0.5 m s^{-1}, which matches favourably with ADCP measurements (Cromwell et al., 1996) and the satellite observations (Fig. 8e,f). Of crucial importance for studies of the SPG is the pathway of the Gulf Stream extension after its separation from the US coast and in particular its retroflection after the Northwest Corner off Newfoundland (50°N–50°W). As seen in the satellite observations the flow in ORCA12 hugs the North West Corner before swerving eastward into the open Atlantic (Fig. 8e–h). This is a key improvement compared to ORCA025 where the North Atlantic Current steers out into the basin interior too far south (Fig. 8e,f). The pathway followed by the North Atlantic Current in ORCA12 appears realistic compared to observations, despite taking a slightly more northward route east of about 30°W.

The Labrador Current is clearly visible in ORCA12, extending well south of Flemish Cap (Fig. 8e,f). This same southward extension of the Labrador Current along the US coast is not found in satellite observations (Fig. 8g,h) but has been observed in hydrographic surveys (Fratantoni and McCartney, 2010). Limitations of satellite altimetry over shelf regions as well as a lower resolution (1/4°) may explain the absence of this feature in Fig. 8g,h. Around Greenland and the Labrador Sea the boundary currents are more pronounced in ORCA12 than in the observations and in the Labrador Sea the current forms a loop whereas altimetry data suggest it should break up along West Greenland before reforming along the Canadian coast (Fig. 8e–h). This suggests that the West Greenland Current is too stable and no eddies are formed along its pathway. This could be caused by an inaccurate representation of the complex topography in this area (west of 53°W), since in reality these topographic constraints give rise to destabilisation and eddy formation when the continental slope becomes less steep (Belkin et al., 2009). In ORCA12 a break of the West Greenland Current could also be forced by locally modifying the lateral boundary conditions to either no-slip or partial-slip rather than the free-slip ones that are currently being used (Quartly et al., 2013).

We note here that altimetry data has limitations in its ability to resolve mesoscale features in the SPG region, since the resolution is coarser than the Rossby radius at these latitudes (about 10 km). Nevertheless, the comparison with altimetry suggests that ORCA12 generally shows a realistic shape of the SPG and south of Greenland, and it also exhibits a reduced circulation around Reykjanes Ridge, which is more realistic than the excessively pronounced one found in ORCA025. The more realistic pathway of the North Atlantic Current in ORCA12 largely explains the reduction of the cold temperature bias seen in ORCA025 off Newfoundland (Fig. 4).

This state of the circulation is reached within the first 10 years of simulation.

3.4. Labrador Sea

Labrador Sea (LS) dynamics play a central role in the climate system, being one of the main areas of deep-water formation in the global ocean. Several global climate models develop erroneous salinity patterns across the subpolar region, affecting other properties such as the MLD, which tends to show an unrealistic deepening in the LS for most of these simulations (Rattan et al., 2010; Treguier et al., 2005). We therefore analyse the LS and the adjacent regions in ORCA12, to assess the capability of the model to represent their main hydrographic features.

3.4.1. Mixed layer depth

The ocean mixed layer plays a central role in climate variability, modulating atmosphere–ocean interactions (Carton et al., 2008). Across

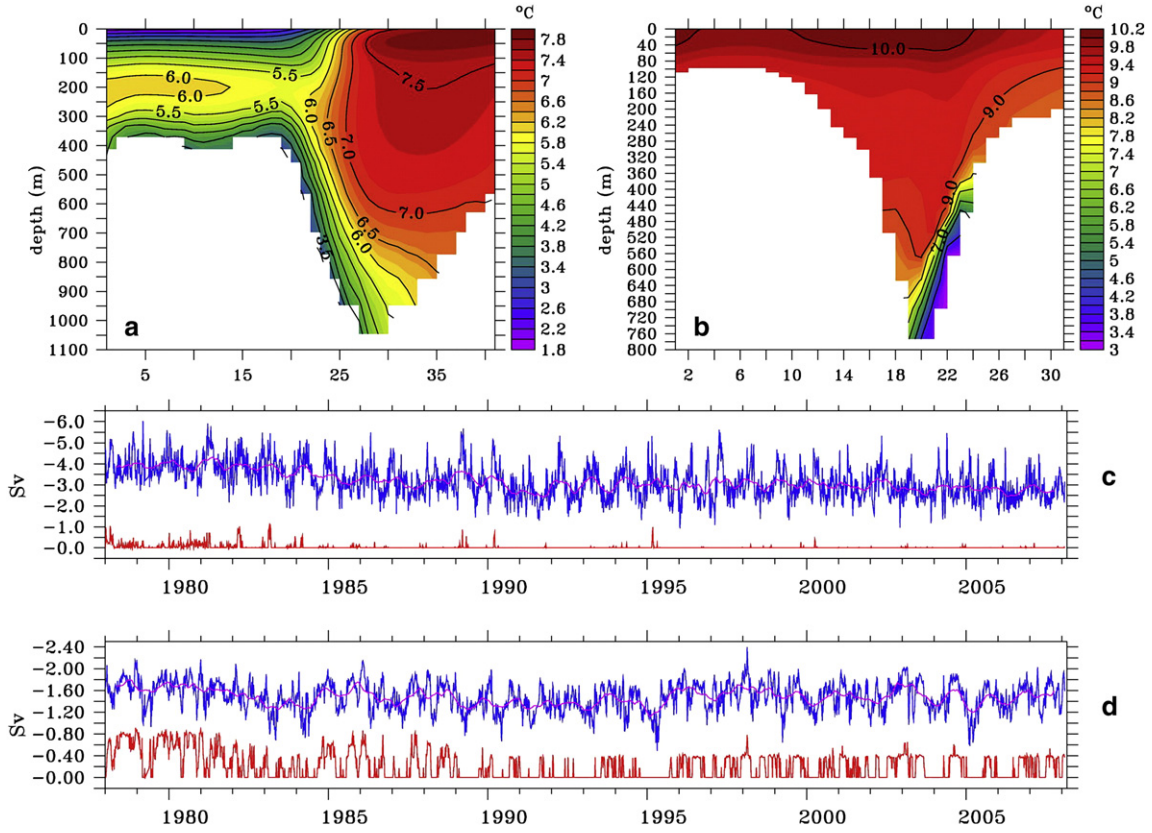

Fig. 7. Top panels: sections from Fig. 6 across the Denmark Strait (a) and the Faroe Bank Channel (b). Shaded are temperature values, used to apply a mask for the calculation of the overflow transport in temperature classes. The horizontal axis is in model indices, representing the width of the section (which is zonal in the Denmark Strait, and meridional in the Faroe Bank Channel). Bottom panels: time series of the overflow volume transport for the whole run, calculated across the sections in the Denmark Strait (c) and Faroe Bank Channel (d). Blue lines correspond to the model temperature classes (5.5 and 7 °C isotherms) from the top panels, red ones to those suggested by observed values (2.5 and 3 °C isotherms). Negative values denote a southward flow across an east–west section in the Denmark Strait and a westward flow across a north–south section in the Faroe Bank Channel.

the analysed North Atlantic domain, the mixed layer is generally represented quite realistically by ORCA12. The spatial pattern of winter MLD, and the absolute values are consistent with observation-based climatologies (de Boyer Montégut et al., 2004). In the LS the spatial pattern is as expected (Fig. 9a); shallower in the boundary currents and areas of deeper mixing (up to 1600–2300 m) in the centre of the Labrador and Irminger Sea gyres (Haine et al., 2008; Yashayaev, 2007). The area of maximum deepening in the simulated LS is shifted slightly northward (around 60°N) and is too deep compared to observations (de Boyer Montégut et al., 2004). In some years the winter mixing almost reaches the seafloor causing excessive and unrealistic mixing of the water column (Fig. 9b). This excessive deepening also characterised the 1/4° resolution version of the model (Rattan et al., 2010), and is a recurrent bias for numerical models in this area (Treguier et al., 2005). Especially during the second part of the simulation, the extent of the area subjected to excessively deep convection in ORCA12 is reduced compared to ORCA025, exhibiting a DWBC that circulates around the regions of deep mixing rather than being part of it. Despite this improvement, convection is still generally too deep and extends too far north in the LS.

ORCA12 shows significant improvements from ORCA025, exhibiting a significant reduction in the extent of the area subjected to excessively deep convection, and a DWBC that circulates around the areas of deep mixing rather than being part of it.

The section taken at 60°N (Fig. 9b) shows how the excessive deepening of the mixed layer is confined to certain years, reaching its maximum depth between 1992 and 1993. The timing of these periods is consistent with observations, which show a period of exceptionally intense convection in the 1990s (e.g. Lazier et al., 2002). During this event there was mixing down to 2300 m in the central part of the basin, triggering the formation of the densest, deepest, and most voluminous LSW ever recorded (Yashayaev, 2007). In the model this period is followed by about five years of restratification, and between 2000 and 2004 there is another episode of intense deep mixing, which is also consistent with observations (Yashayaev, 2007). Fig. 8 of Yashayaev (2007), which analyses data from the AR7W hydrographic section, shows the thickness of two LSW vintages. The data exhibit deep MLD in the early 1990s (peak of 2100 m in 1994), as does the model, followed by a period of shallower MLD, before renewed deeper mixing in 2000–2001 (peaks of 800–900 m); the model is characterised by a similar pattern (Fig. 9b), but the maximum mixing is higher in each case (3400 and 2600 m, respectively). The AR7W hydrographic section extends diagonally across the basin, from the Labrador Peninsula to the western coast of Greenland. This crosses the model 60°N section obliquely, passing through a region where model mixing reaches on average 1200–1600 m (green and yellow colours in Fig. 9a, which is closer to observed values. However, the mapping of LSW thickness in Yashayaev (2007) also shows that there is no equivalent region of greater LSW thickness northwest of the AR7W section. Finally, the simulated convection in the Labrador and Irminger Seas is in phase only at certain times (especially between 1985 and 1995), and generally exhibits lower values in the Irminger Sea (Fig. 9b).

3.4.2. Hydrographic structure

A further common inaccuracy in global models is excessive warming and salinification of the Irminger and Labrador Seas (Rattan et al., 2010; Treguier et al., 2005). We explore this behaviour in ORCA12, by analysing the evolution of temperature and salinity across the section

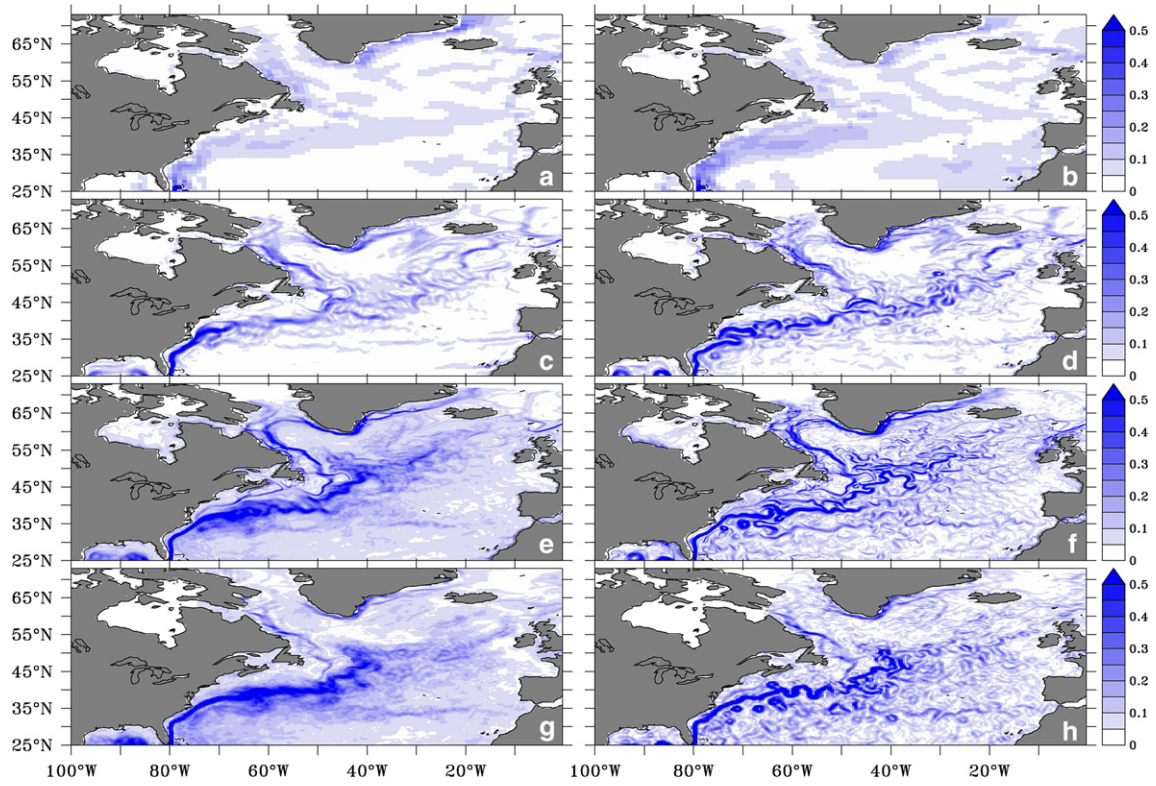

Fig. 8. Surface velocity in ORCA1 (a,b), ORCA025 (c,d), ORCA12 (d,e) and geostrophic velocities inferred from satellite altimetry (g,h). Units are m s^{-1}. The left column shows annual mean values for 2007 (last year of the model simulations). The right columns show a 5-day average for the three model resolutions and a weekly average for the satellite based geostrophic velocities.

at 60°N both in the central LS (57°W), and in the core of the West Greenland boundary current (47°W).

The bottom of the LS is characterised by waters originating in the Nordic Seas, below 1.8 °C and 34.9 g kg^{-1} (Yashayaev, 2007), and the model LS does exhibit these values at the beginning of the run. However, by the end of it, both temperatures and salinities below 200 m show significantly higher values (Fig. 10). Deep waters and intermediate to shallow waters evolve differently. In the central LS, deep waters (below ~2500 m) show a slow but constant increase from initial conditions in temperature and salinity (after initial cooling). By the end of the simulation they have increased by ~1 °C and almost 0.1 g kg^{-1}, respectively. Intermediate to shallow waters exhibit increasing temperature values after 1997, following initial moderate cooling (Fig. 10a). Salinity values are characterised by a constant increase throughout the whole run, which is somewhat accelerated after 1995 (Fig. 10b).

The West Greenland boundary current (BC) also exhibits an initial cooling until 1995 in the top 1000 m (Irminger Water), followed by a period of warming. The deeper layers (Nordic Sea overflow water) show a slow but constant increase throughout the simulation, after slight cooling during the first year (Fig. 10c). In the depth range 200–1500 m the increase in salinity values is slow but constant across the whole water column, with an acceleration after 1995 (Fig. 10d). The model's BC is therefore too warm and saline, which suggests that it does not contain sufficient cold fresh Arctic-origin water. The warming of bottom waters is faster in the central LS than in the BC, suggesting that the BC is not entering the LS at the correct rate. Observations show an increase in temperature at 200–1500 m depth after 1995 (Yashayaev, 2007), but the model's rate of change (and the mean) is higher.

The temporal changes in the central LS are similar to those in the BC (Fig. 10e and f). Temperatures consistently increase throughout the simulation both in the BC and in the central LS; there is an increase of this temperature difference after 1990 just prior to the onset of the LS and BC warming described earlier. This covariance at the two locations suggests that temperature and salinity variability in the central LS may originate in the BC. Salinities exhibit an almost monotonic increase both in the central LS and in the BC, which gradually plateaus towards the end of the run at both locations. It is likely that this long-term salinity trend reflects a model drift rather than a real signal, and may result from insufficient input of fresh water from the shallow Arctic outflows. The salinification drives excessive convection and masks the real interannual variability (Rattan et al., 2010). Insights on the possible sources and potential consequences will follow in the discussion. The interannual variability simulated for the temperature evolution in the central LS and BC is more likely to be representative of documented changes in the North Atlantic SPG. Previous studies have shown that the mid 1990s coincide with the warming of the whole subpolar region (Robson et al., 2012a; Stein, 2005), and Fig. 10 provides some insight about the possible timing of this warming event in the LS.

3.4.3. Boundary currents

The capability of the model to resolve boundary currents has been assessed by comparing the modelled meridional velocity field of a section across the Labrador and Irminger Seas with observations (Fig. 11). The observed data (Fig. 11a) have been collected during a cruise in August–September 2008, and the parameter shown is velocity normal to the section (geostrophic velocities corrected with LADCP). The model data for the same period (August–September 2008) is shown in (Fig. 11b). The simulated western boundary currents are continuously present in the Labrador and Irminger Seas, in the same locations, of similar width, and characterised by velocities generally close to observations. In the Irminger Sea, the depth reached by the boundary current is very close to observations (down to ~2000 dbar), but below 1000 dbar the velocities are higher in the model. The modelled West Greenland Current appears too shallow in the eastern LS, with the main core of the current only reaching down to ~1500 dbar, instead of

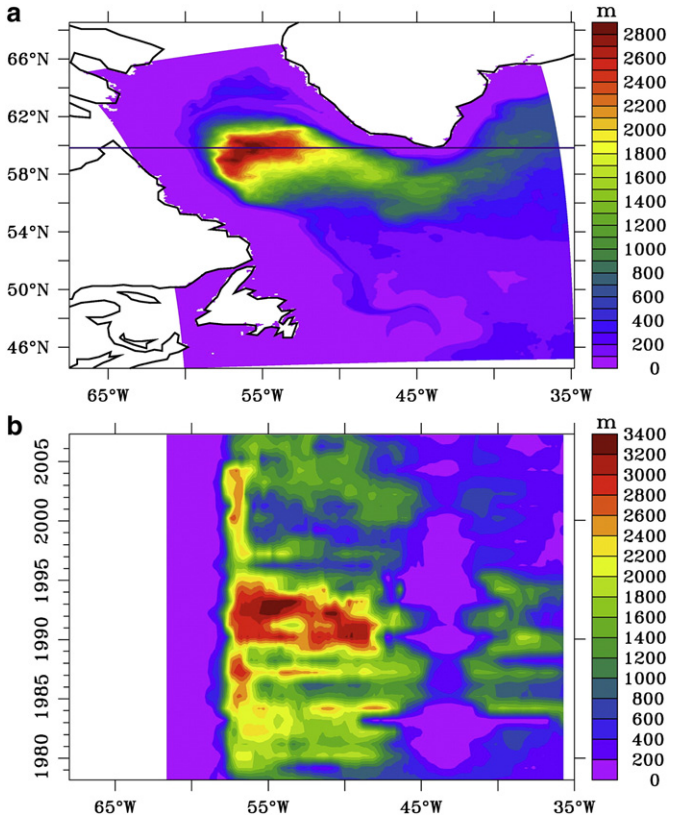

Fig. 9. (a) Winter mixed layer depth climatology in the Labrador Sea and part of the Irminger Sea, averaged over the last 25 years of run, for the months of March and April. (b) Hovmöller diagram of the mixed layer depth evolution throughout the simulation, across the section indicated by the black line in panel a, for the March–April period.

the observed 2800 dbar (but there is still weak northward flow to the bottom). This is typical of z-level models (with prescribed depth levels), which tend to have too shallow representation of the circulation (Pacanowski and Gnanadesikan, 1998). In the Irminger Sea, the depth reached by the boundary current is very close to observations (down to ~2000 m), but below 1000 m the velocities are higher in the model. The shallow western boundary current in the model is too wide (~150 km in the model compared to ~50 km in the data), especially in the Labrador Sea, and while high velocities extend too deep, the velocities at water depth 1500–3000 dbar are realistic.

With the presence of significant spatial and temporal variability it is important to understand whether these 60-day segments are representative of the mean circulation. There is only one example of long-term, full depth observations available across the full width of LS (Hall et al., 2013). Both these 6-year LADCP measurements and the 2008 hydrographic section presented here portray the highly barotropic structure of the flow along the section, similar circulation patterns, and velocity values. The August–September 2008 velocity field is also entirely consistent in structure and velocity (± 0.02 m s^{-1}) with the Irminger Sea multi-year mean velocity field shown in Våge et al. (2011). The August–September 2008 model velocity field is also consistent with the annual mean from the same year in the model (Fig. 11c); the boundary currents are very similar in location, width, depth and velocity. The biggest difference is in the recirculation adjacent to the West Greenland Current. From this we assert that although the observations are from a synoptic survey, the comparison with the model is valid and useful.

3.5. Barotropic and meridional overturning stream function

The combination of the barotropic and meridional stream functions provides an invaluable tool to analyse the dynamics and evolution of ocean circulation in numerical models. First we calculated the barotropic stream function (Ψ_B) for the last 25 years of the run (Fig. 12a) to better assess how the model simulates the main features of the SPG. This defines the depth-averaged flow v (where v is the meridional velocity component) and is calculated as:

$$\Psi_B(x,y) = \int_{x_w}^{x} dx \int_{-H}^{0} dz\ v(x,y,z),$$

where x_w is the starting point of the integration (on land), H is the ocean depth and x and y are the longitudinal and latitudinal directions of the model grid.

The circulation in the North Atlantic consists of two gyres, the anticlockwise SPG to the north (corresponding to negative stream function values) and, partially visible to the south of the analysed domain, the Subtropical Gyre (Fig. 12a) with clockwise rotation (positive stream function values). Several other large scale features typical of this region can be easily identified, such as the pathway of the Gulf Stream, along which the highest values of northward transport (over 25 Sv) can be found, and the full shape of the SPG, showing transports of up to 45 Sv in the LS. The mean transport in the Florida Strait is slightly underestimated by ORCA12 compared to observations (as discussed by Blaker et al., 2014). Observed values for the transport in the LS are not available for comparison, apart from a single transport estimate in 2008 across the LS, measuring a maximum of 40 Sv (Hall et al., 2013). Model results can also be compared to measurements of the transport in the western boundary current in the Irminger Sea provided by Våge et al. (2011) (32 ± 4 Sv). In both cases, these are not directly comparable to the model mean but show lower transport values.

The structure of the circulation in the North Atlantic can also be analysed through the overturning stream function (Ψ), which is calculated as:

$$\Psi(y,z) = \int_{x_w}^{x_e} dx \int_{z}^{0} dz'\ v(x,y,z'),$$

where z is the ocean depth (the surface is at $z = 0$), and x_w and x_e represent the starting points of the integration (both on land). In this case the integration is carried out across the Atlantic.

The AMOC consists of a northward surface flow in the top 1000 m, sinking between 45 and 65°N, and a southward return flow mainly occurring between depths of ~1000 and 3000 m, with some southward flow related to the Antarctic Bottom Water found down to depths of 4500 m (Fig. 12b). The maximum AMOC values of 18 Sv are found at ~900 m depth (around 35°N) and they compare favourably with the observed time series inferred from the RAPID/MOCHA array at 26.5°N between 2004 and 2008, which exhibit an annual maximum overturning transport of 18.7 Sv (Cunningham et al., 2007; Kanzow et al., 2010; McCarthy et al., 2012; Rayner et al., 2011). The evolution of the AMOC at 26°N exhibits an initial strengthening of the cell (picking up in the first 10 years of the run), but also a clear weakening after 1995 which is in broad agreement with the observed decline since 2004 (Smeed et al., 2013), with maximum values decreasing from 21 Sv (reached in 1986, 1988, and 1994) to 16 Sv, centred at a depth of ~800 m (Fig. 13a). The highest values of southward transport (absolute values) are reached between 4000 and 4800 m, with a peak in 1997–1998 (7 Sv). The strength of the AMOC at 26°N has also been calculated both at the beginning and at the end of the simulation (Fig. 13b) for a clearer comparison. The northward transport between 500 and 1500 m is clearly weakening throughout the run, while the southward transport at greater depths is strengthening, with differences up to 2 Sv in both cases. A recent study by Duchez et al. (2014) also shows

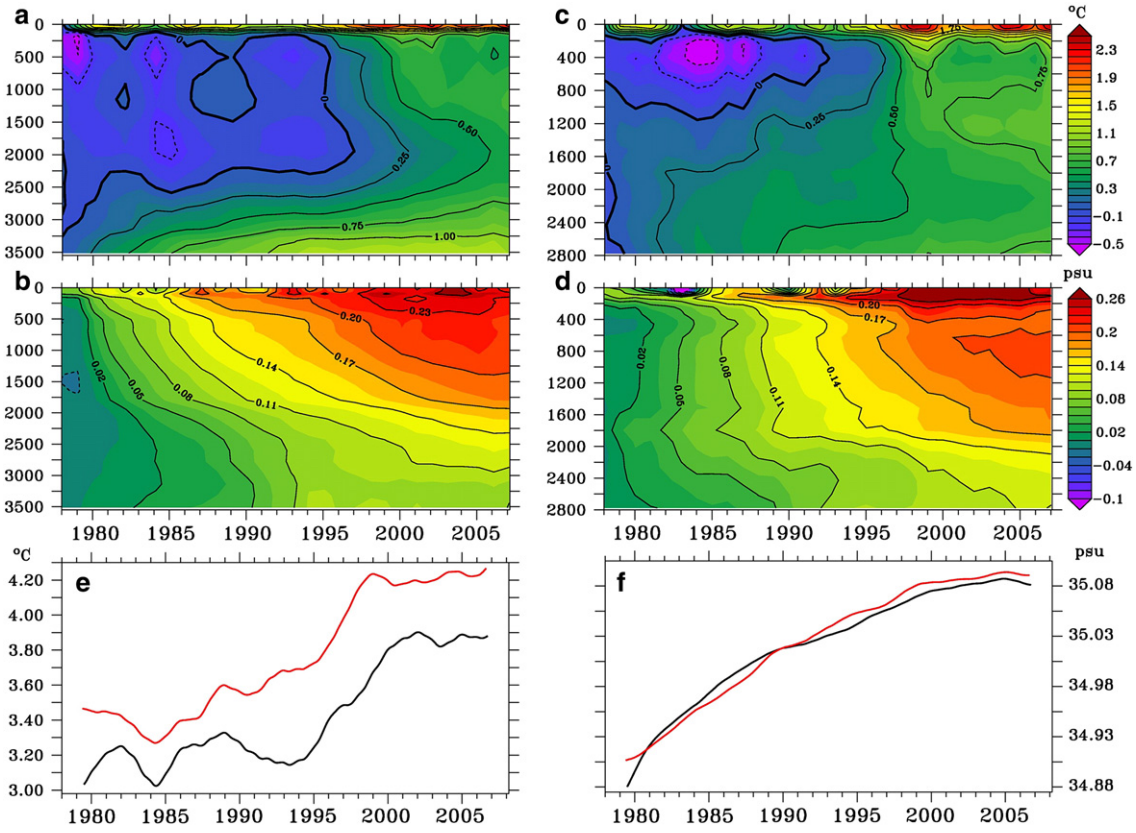

Fig. 10. Top and middle panels: Hovmöller diagrams of temperature (a,b) and salinity (c,d) anomalies (from the first month of simulation) in the central Labrador Sea (60°N, 57°W, a and c) and in the West Greenland boundary current (60°N, 47°W, c and d). Bottom panels: evolution of temperature (e) and salinity (f) values throughout the run. Black lines represent central Labrador Sea Water, and red ones correspond to the core of the West Greenland boundary current (in both cases, values are averaged between 200 and 1500 m).

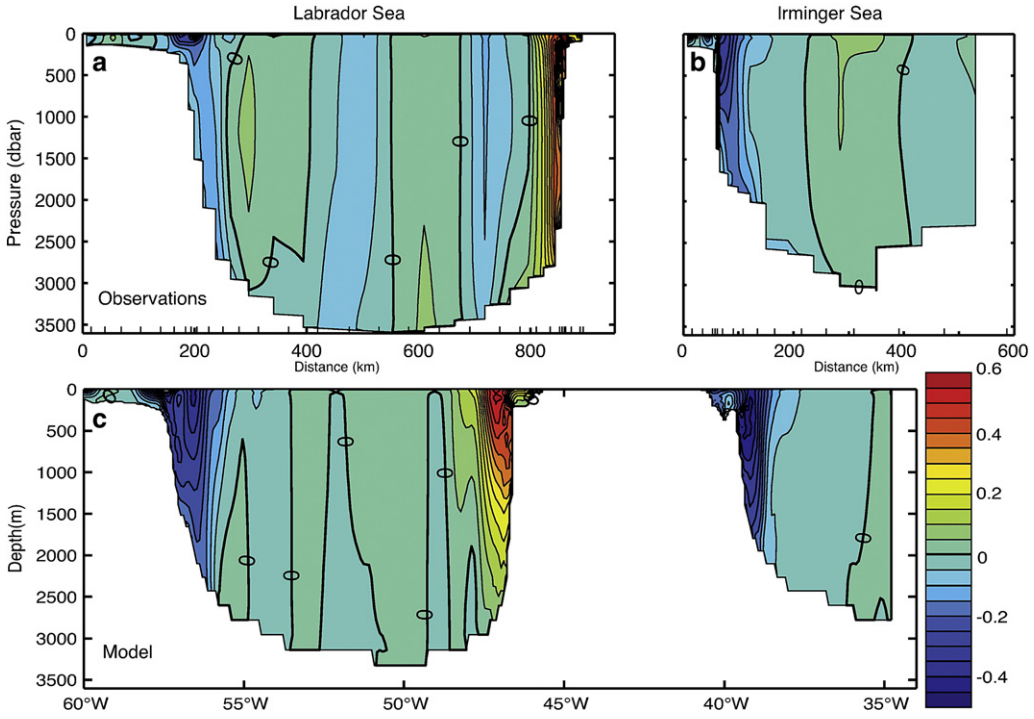

Fig. 11. Sections across the Labrador Sea and part of the Irminger Sea, showing the structure of the boundary currents. Comparison between measurements of geostrophic velocities corrected with LADCP in August–September 2008 (top panels) and ORCA12 meridional velocities in 2008, averaged over the same time period (middle panel) and an annual mean for 2008 (bottom panel). The exact locations of the hydrographic sections across the Labrador and Irminger Seas can be found in Bacon (2010) and Fig. 1 shows where the section was taken in the model.

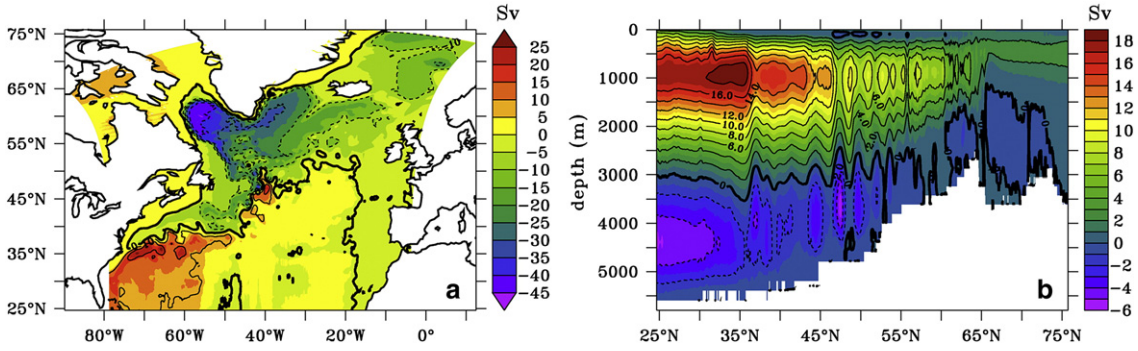

Fig. 12. Barotropic (a) and meridional overturning (b) stream function values shown by shading and contours. The meridional overturning stream function is a zonal integral of the Atlantic basin, and the barotropic one is shown for the whole analysed domain; in both cases, a mean of the last 25 years of the run is shown. Values are expressed in Sverdrups, where: 1 Sv = 10^6 m^3 s^{-1}.

that ORCA12 represents the observed seasonal cycle in the AMOC very realistically.

3.6. Evolution of the North Atlantic subpolar gyre

In a numerical model the best way to obtain a SPG index is to use the barotropic stream function (BSF), given that it represents the volume transport between any two points in the ocean. We therefore define our SPG index by calculating the minimum BSF at 60°N, to analyse the evolution of the SPG in the run (Fig. 14a). To better compare this with previous studies, we also compute the meridional overturning stream function at 26°N (Fig. 14b) to show the evolution of the AMOC during the simulation. Both stream functions have an increasing trend (in terms of absolute values) in the first eight years of the simulation which is followed by different oscillations until 1995. After this year, both the SPG and AMOC indices exhibit a pronounced decreasing trend until 2005, when they start increasing again. This is consistent with previous studies that showed the same weakening trend during the mid to late 1990s (Gao and Yu, 2008; Häkkinen and Rhines, 2004; Hátún et al., 2005). The maximum strength of the BSF is reached around 1985 and 1994, with values ranging between 76 and 78 Sv. The highest values of the AMOC are ~20 Sv, and they are reached during three main peaks between 1985–1986, 1988–1989, and 1994–1995.

Both stream functions exhibit minimum absolute values (~53 Sv for the BSF, and 15 Sv for the AMOC) at the beginning of the simulation and again around 2005, following the consistent weakening from 1995 onwards. The weakening trend in the subpolar circulation has also been found in previous studies (Hátún et al., 2005) and coincides with a period of rapid warming that characterised the SPG in the mid 1990s (Robson et al., 2012a; Stein, 2005), during which this region warmed by more than 1 °C. The possible causes of this warming as well as its predictability have been the subject of recent studies that suggest that changes in the ocean circulation played a major role (Robson et al., 2012a,b). The current view is that the SPG warming event was preceded by a prolonged positive phase of the North Atlantic Oscillation (NAO) that led to an anomalously strong AMOC and therefore to a strong oceanic meridional heat transport (MHT). ORCA12 can provide further insight into the spatio-temporal development of the SPG warming event (Fig. 15).

The comparison between the evolution of SSTs in ORCA12 and in observations (NOAA optimal interpolation dataset, Reynolds et al. (2002)) reveals a characteristic pattern for the SPG warming. The warming starts in the southernmost part of the SPG in 1994 and within two years (1996) the warm anomaly spreads into the eastern part of the SPG. After about 4 years (1998) the warm anomaly reaches its maximum amplitude and encompasses the whole SPG, including the LS. By 2000 the amplitude of the SPG warm anomaly rapidly reduces and the anomalously warm waters are exported along the Canadian and U.S. east coast. There is remarkable agreement between the modelled and observed evolution of the SPG warming (Fig. 15). This is not an obvious result, given that as previously mentioned the warming event cannot be explained by air–sea interactions alone.

4. Discussion

The comparison between ORCA12, ORCA025 and ORCA1 demonstrates the improvements provided by the increase in resolution. Using the FLAME (Family of Linked Atlantic Model Experiments)

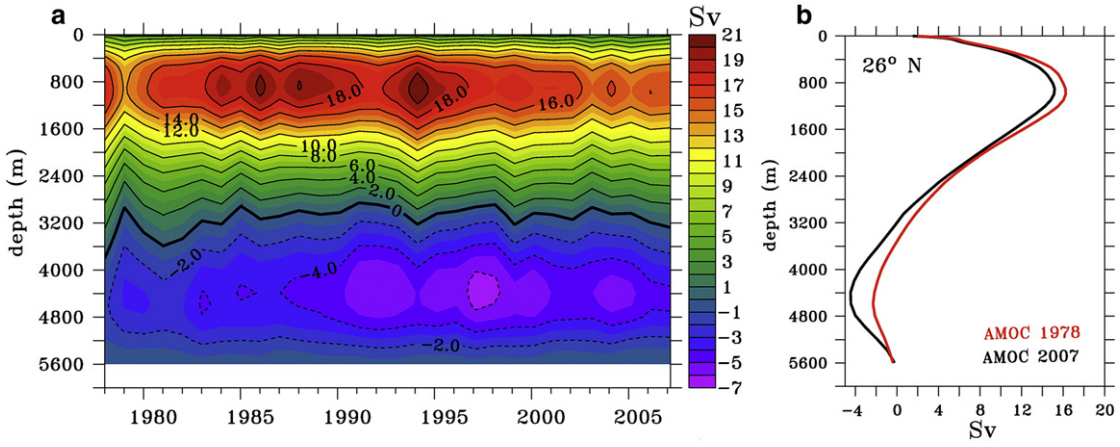

Fig. 13. Left panel: Hovmöller diagram of the AMOC at 26°N (a) for the whole simulation. An annual filter is applied. Right panel: annual means of AMOC values at 26°N (b). The red line is the first year of the run (1978), and the black line is the last year of the analysed simulation (2007).

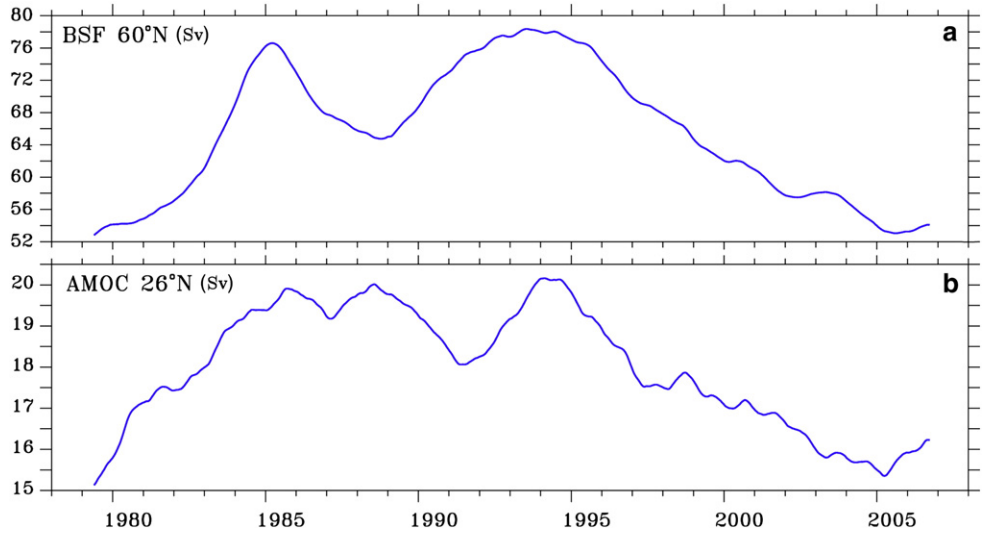

Fig. 14. Minimum barotropic stream function, representing the North Atlantic Subpolar Gyre Index (a), and maximum AMOC at 26°N (b) calculated for ORCA12.

model Eden and Böning (2002) also demonstrated remarkable advancements in the simulation of circulation patterns in the SPG when considering eddy resolving versions. However, in contrast to our study, the FLAME configurations are regional (20°S to 70°N) and strong restoring towards climatological values is applied for temperatures and salinities at the northern and southern boundaries of the domain. Even in the state-of-the-art versions, the representation of some of the key features of the SPG remains challenging for most OGCMs, as demonstrated by some local erroneous features and on-going drifts still found in ORCA12.

The drifts associated with bottom water properties in the LS are likely linked to the simulation of the overflow waters (Danabasoglu et al., 2010; Zhang et al., 2011). Whereas the overflow strength in the model compares rather well with observations, the overflow waters in ORCA12 are too warm and saline. To correct this bias it might be necessary to apply a physical parameterization for the Nordic Seas overflows.

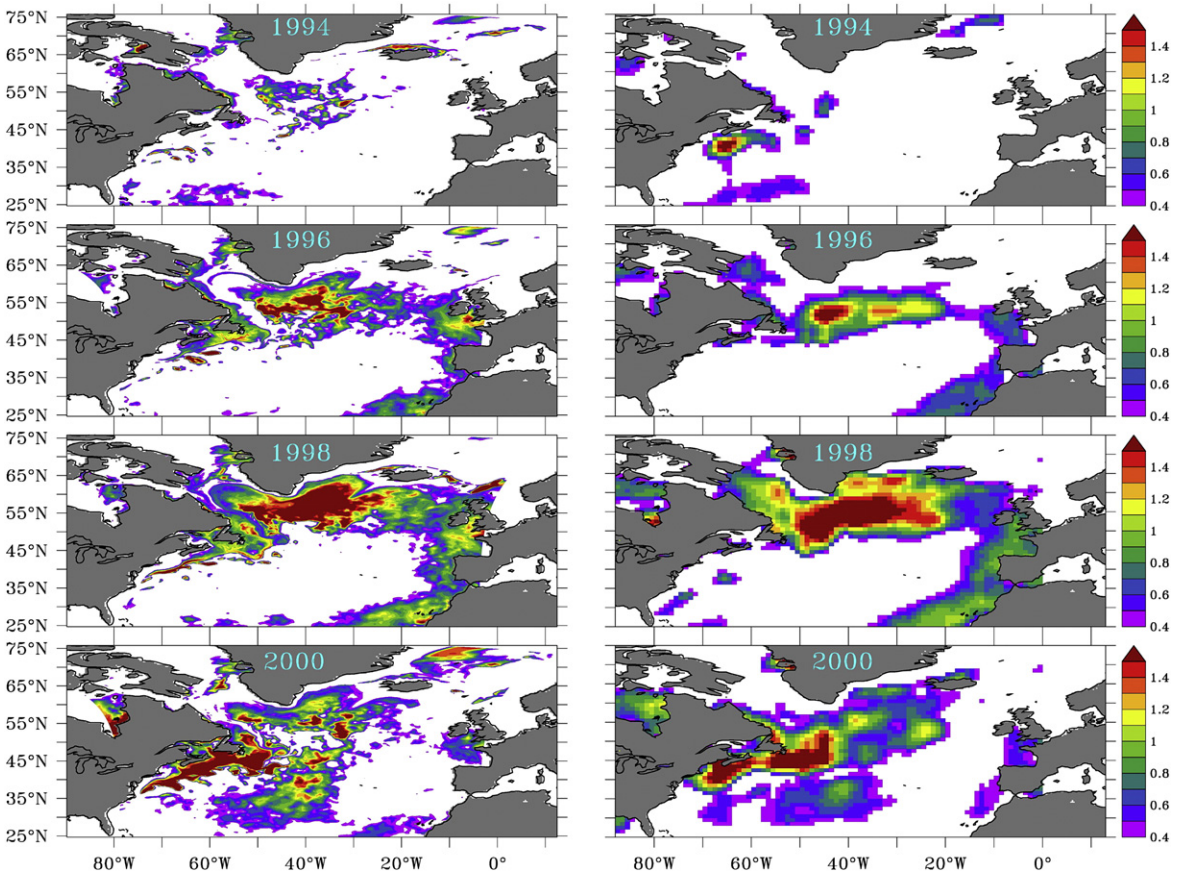

Fig. 15. Warming of the Subpolar Gyre in ORCA12 (left panels) and in the NOAA optimal interpolation SST dataset (right). Units are °C and only positive temperature anomalies larger than 0.4 °C are contoured.

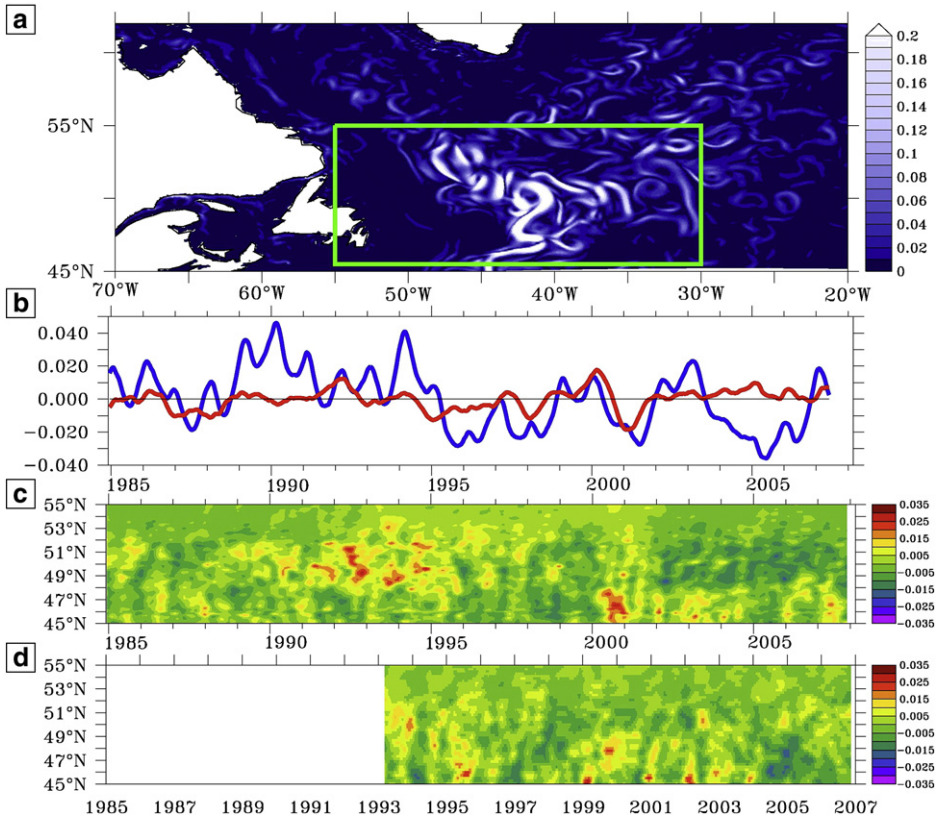

Fig. 16. a) Snapshot of eddy kinetic energy (EKE) in ORCA12; the green box denotes the area over which the kinetic energy is zonally averaged (see panels c and d). b) Zonal (blue) and meridional (red) wind stress anomalies (with respect to 1989 to 2001) averaged over the region delimited by the green box shown in panel a. Units for wind stress are N/m^2. Units are cm^2/s^2. c) Zonally averaged kinetic energy in ORCA12 (cm^2/s^2). The mean for the 1985 to 2007 period has been subtracted. d) Zonally averaged kinetic energy obtained from AVISO geostrophic velocity anomalies (cm^2/s^2). The mean for the 1993 to 2007 period has been subtracted.

In particular, the dense overflow in the Denmark Strait, directly south of the sills, tends to mix rapidly with lighter ambient waters, leading to an underestimation of the maximum density found in the Irminger Basin (Beismann and Barnier, 2004; Willebrand et al., 2001). This behaviour is common for many ocean models, especially for those using a stepwise representation of the bottom topography (Beismann and Barnier, 2004; Willebrand et al., 2001), which is also used in ORCA12.

Parameterising the overflows from the Nordic Seas is not the only suggested way to achieve a more realistic hydrographic structure in the LS. Here eddies are a prominent mesoscale feature of the circulation, being crucially important in the restratification of the interior of the basin after deep convection and modulating the temporal variability of deep-water formation (Gelderloos et al., 2011). In the real ocean these eddies are of three types (Gelderloos et al., 2011) and particularly the West Greenland Current eddies that shed off Cape Desolation appear critical for preconditioning LS convection, as they contribute to the restratification of the water column in the summer months, limiting deep convection the following winter (Chanut et al., 2008). ORCA12 is able to reproduce most of the eddy activity and recirculation in the Labrador and Irminger Seas, but it cannot simulate enough local eddies in the LS (see Fig. 8). This problem could be solved by locally changing the lateral boundary conditions from free-slip to no-slip. No-slip conditions have been shown to increase eddy formation by destabilising boundary currents (Quartly et al., 2013). Ultimately, an adequate representation of local eddies could correct the overestimation of the winter MLD in the Labrador Sea area (Talandier et al., 2014).

LS dynamics and deep-water formation directly determine the strength of the AMOC (Döscher and Redler, 1997), which reacts with a delayed enhancement (with a time lag of 2–3 years) to anomalous deep convection in the LS (Eden and Willebrand, 2001; Gulev et al., 2003). The instantaneous response to fluctuations in the wind-stress forcing and the delayed reaction to changes in the wind-stress field results in an enhancement of both the STG and SPG circulation (Beismann and Barnier, 2004; Eden and Willebrand, 2001; Gulev et al., 2003). This might explain why AMOC values in ORCA12 are sometimes slightly higher than the observations, as a response to the excessively deep convective events in the LS, which can be observed in the first part of the run (first 10–12 years), when convection in the Labrador and Irminger basins is particularly intense. In the second part of the simulation the strength of the AMOC is gradually decreasing and so is the intensity of the convection in the LS.

Years exhibiting the deepest mixing in the LS generally correspond to those characterised by intense convection also in the real ocean (even if values tend to be higher in the model), which reflects a good response of the model to the surface forcing. This is also shown by the SPG index calculated for ORCA12 (Fig. 14a), which exhibits very similar trends between 1980 and 2007 compared to other SPG indexes based on altimetry and modelled data (Hughes et al. (2012), extended after Hátún et al. (2005), Fig. 2b). Significant changes occurring in most of the analysed fields from 1995 onwards are also a result of the realistic response of the model to the forcing, which reflects the period of warming experienced by the North Atlantic during the 1990s, triggering changes in the circulation and a weakening of the SPG. This is shown by the decreasing trend in the index after 1995, and the subpolar circulation seems to be regaining strength only after 2005, marked by the return of an increasing trend in the SPG index, in accordance with the observed deep convection in the subpolar North Atlantic in winter 2007–2008 (Våge et al., 2009). Interestingly, after 1995 the same trends can be tracked in the AMOC at 26°N.

In ORCA12 the western boundary currents are clearly present in the Labrador and Irminger Seas and characterised by velocities generally close to observations (Figs. 8 and 11). The shape of the SPG is more

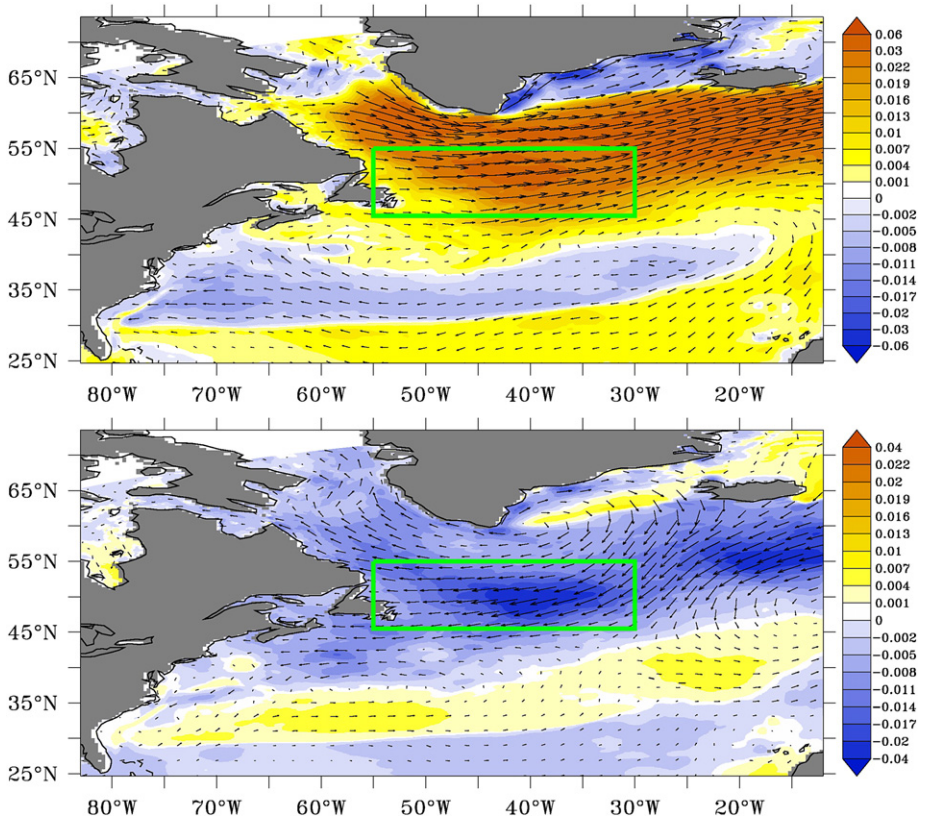

Fig. 17. Wind stress anomalies averaged across the area indicated by the green box, over the periods 1989–1995 (top) and 1995–2001 (bottom). Anomalies are computed with respect to the period from 1985 to 2007 and shading indicates the amplitude of the wind stress anomaly in N/m^2. Arrows indicate the pattern of the anomalous wind field.

realistic in ORCA12 than in ORCA025 and ORCA1, with a marked improvement off Newfoundland where the Gulf Stream extension now follows the Northwest Corner rather than steering out into the open ocean too far south as seen in ORCA025 (Fig. 8). The improvement in the simulation of the Gulf Stream and the NAC when going from eddy permitting to eddy resolving (1/10°) models was first documented by Smith et al. (2000) and a better representation of the pathway of these currents with increased resolution was also found in a regional version of the model, NATL12 (Treguier et al., 2012).

Of particular interest, is the ability of ORCA12 to reproduce the spatio-temporal structure of the SPG warming observed in the mid 1990s (Fig. 15). This event was due to both air–sea fluxes and to changes in ocean circulation (Robson et al., 2012a) and the good agreement of the SST evolution in both model and observations suggests that the contribution of ocean dynamics to the SPG warming is realistic in ORCA12. In particular, the model can provide additional insight into how the ocean transports heat into the interior of the SPG. An increase in AMOC (MHT) across a given longitude–depth section is consistent with an increased ocean heat content (OHC) north of that section (e.g. Bryden et al., 2014; Sonnewald et al., 2013). However, an increase in the AMOC (and MHT) to the south of the SPG does not explain how the excess of heat can reach the interior of the SPG. Rather than warming the SPG it is also conceivable that the increased MHT would heat the region east of the SPG instead. Furthermore, the fraction of the total ocean MHT that is due to the AMOC decreases with increasing latitude and north of about 50°N the largest fraction of the MHT is actually linked to the horizontal circulation rather than with the AMOC (e.g. Marsh et al., 2009; Gulev et al., 2003). One could therefore expect the warm anomaly to first follow the NAC and the East and West Greenland Currents before gradually spreading into the interior of the SPG. However, this is unlikely to be the case, since the temperature anomalies along Greenland are smaller than in the interior SPG (Fig. 15, years 1996 and 1998).

One process that contributed to the warming of the SPG interior is variability in eddy activity at the intergyre boundary between the STG and the SPG (Häkkinen et al., 2013). The eddy kinetic energy (EKE = $\left((u-\bar{u})^2+(v-\bar{v})^2\right)/2$, where $\bar{u}$ and $\bar{v}$ are the time mean) in ORCA12 suggests that the SPG warming was preceded by a phase of increased eddy activity at the southern tip of the SPG from the late 1980s to about 1995 (Fig. 16). This increase is most clearly seen between 1990 and 1996 between 47°N and 53°N and tails off towards the late 1990s. The increased eddy activity that happened before and during the early stages of the SPG warming is consistent with an enhanced mixing of warmer waters into the SPG interior. No observations of the ocean mesoscale eddy activity are available prior to 1993 so we cannot determine if the increase in activity from the late 1980s onwards that we see in ORCA12 is a realistic feature. However, from 1993 onwards we can use geostrophic velocities derived from satellite altimetry to estimate the EKE in the real ocean. The observations suggest a decline in eddy activity between 47°N and 53°N that is comparable to that seen in ORCA12. Despite differences between ORCA12 and the satellite derived observations for the 1993 to 2007 period, the temporal evolution is generally similar in both datasets. This gives us some confidence that the increase in eddy activity simulated in ORCA12 prior to the SPG warming could be representative of the behaviour of the real ocean.

Zonal wind stress anomalies (with respect to 1989 to 2001) averaged over the southern SPG box (Figs. 16 and 17) show that the increase in mesoscale eddy activity simulated between the late 1980s to mid-1990s coincides with a strengthening of the westerly wind component over the southern part of the SPG. The zonal wind stress averaged over the southern SPG box (Fig. 16) shows maximum values during the period of maximum EKE at the intergyre boundary. Minimal change

in the strength of the meridional wind component occurred during the same period, but an abrupt decrease in the zonal wind stress occurs in the mid 1990s, and thereafter the zonal wind stress varies around a lower mean. The period from 1989 to 1995 is characterised by a positive wind stress anomaly (with respect to 1989–2001) over most of the SPG, which extends further eastwards towards Europe (Fig. 17). This reflects the positive state of the NAO during these years and the stronger than average westerlies over the North Atlantic. Between 1995–2001 the wind stress anomaly is mainly negative between 45°N and 65°N. The spatial pattern is not purely a mirror image of the pattern seen between 1989 and 1995, and the largest (negative) anomalies are concentrated in a narrow band oriented SW to NE starting at the southern SPG tip off Newfoundland. We note that 1995 coincided with the end of a prolonged period of increasingly positive NAO values that started in the 1980s. Since 1995 the NAO has been a succession of shorter positive and negative phases with no preferred state over longer (i.e. interannual and longer) periods.

Variability of the mesoscale eddy activity on seasonal to interannual timescales in response to wind forcing has previously been suggested by other authors (Biri, 2013; Chelton and Xie, 2010; Garnier and Schopp, 1999; Penduff et al., 2004; Stammer and Wunsch, 1999; Stammer et al., 2006). Bower and von Appen (2008) also suggested a possible link between the North Atlantic Oscillation (NAO) and single or double branch modes of the North Atlantic Current at the southern tip of the SPG. Penduff et al. (2004) linked the variability of the NAO to changes in the EKE in the STG and SPG. These authors showed a reduction in the EKE difference between STG and the SPG in the mid 1990s, followed by a recovery in the late 1990s. Especially during periods of large EKE fluctuation the results suggested a link between the state of the NAO and EKE, supporting an earlier hypothesis by Stammer and Wunsch (1999). A more general link between atmospheric modes of variability and oceanic EKE was recently described by Biri (2013). However, the precise mechanisms through which wind variability can affect the ocean mesoscale eddy activity such as the one observed at the STG/SPG boundary are not yet fully understood. On seasonal timescales Garnier and Schopp (1999) suggest that EKE changes are induced by changing Sverdrup transports and Penduff et al. (2004) argue that on interannual timescales the wind energy input into the ocean (in particular the difference in energy input between the STG and SPG) is a determining factor through which the wind affects the EKE variability.

Quantifying the impact of the increased eddy activity on the SPG warming in our model run would require a heat budget analysis of the SPG with a breakdown of the heat exchange into air–sea fluxes, advective, eddy and diffusive ocean heat transports to conclusively establish the relative contribution of each component. This is beyond the scope of the present paper where the main goal it is to show the performance of ORCA12 in the SPG region. A full budget analysis of this region will be part of a future study and could be directly compared to the results of Desbruyères et al. (2014). Nevertheless, based on the EKE analysis we can hypothesise that an increased eddy activity in the southernmost part of the SPG provided a gateway through which the SPG warmed. To our knowledge such a mechanism has not been described before, but both ORCA12 and the observations suggest that it could have contributed to the SPG warming event in the mid 1990s.

During this event the strong meridional temperature gradient between the cold SPG interior and the northern branch of the Subtropical Gyre was reduced. This likely had repercussions on the atmospheric circulation. As mentioned earlier, the SPG warming was preceded by a long phase of sustained positive NAO, which ended in the second half of the 1990s. The NAO has since been more variable, exhibiting positive and negative years; therefore, the reduction found in the meridional SST gradient between mid and high latitudes of the western North Atlantic that coincided with the SPG warming likely led to a reduction in the baroclinicity for the atmospheric circulation and to a weakening of the North Atlantic Storm Track (Brayshaw et al., 2011; Buchan et al., 2014). Therefore, the increased eddy activity in the southern part of the gyre in the early 1990s and the subsequent SPG warming might have been a contributor to the increased occurrence of negative NAO phases experienced since the mid 1990s.

5. Summary and conclusions

We have presented an overview of the performance of a global eddy-permitting (1/12°) version of NEMO in the subpolar North Atlantic. We have carried out both quantitative and process-oriented validations in this area, and the comparison of model outputs with observations and other modelling studies has allowed us to assess the capability of ORCA12 to simulate realistic conditions in this region. The analysis of the first 30 years of run has highlighted several improvements from the equivalent lower resolution versions of the model, ORCA025 and ORCA1. However, the representation of some key processes in the North Atlantic subpolar regions still presents challenges for global ocean models. We can therefore conclude that, compared to lower resolution versions, ORCA12 exhibits:

- Improvements in the general structure of the circulation in the North Atlantic, especially at the surface, with currents simulated in the correct locations, and following realistic pathways. In particular, the more realistic path of the NAC leads to a more realistic shape of the SPG which coincides with a marked reduction in the SST bias off Newfoundland.
- The volume transport of the Denmark Strait and Faroe Bank Channel overflows is comparable to the observed values. However, the modelled overflow waters are still too warm and too saline.
- Instances of deeper convection in the modelled Labrador and Irminger Seas correspond to years when deeper convection was observed in the real ocean. This suggests that the model is responding well to interannual variability in forcing, despite the fact that the base of the mixed layer is still too deep on average.
- Formation of Labrador Sea Water with realistic features at shallow and intermediate depths, matching favourably with observations, but still showing temperature and salinity biases in the bottom layers with waters getting too warm and too salty.
- A good representation of boundary currents, even if observations suggest that the flow should be more barotropic. A tendency for currents to be too shallow is a typical feature of z-level models like the one we used in this study.
- Good potential for its application in the design of monitoring strategies in the North Atlantic, where ORCA12 could effectively be used to test hypotheses, and analyse key processes for future predictions. For instance, ORCA12 can be used to provide insight into the spatio-temporal development of the warming of the SPG in the mid 1990s.

Acknowledgements

The authors are grateful to K. Jochumsen and B. Hansen for providing updated datasets for the overflows and thank A.-M. Treguier and three anonymous reviewers for insightful comments. A.M. thanks D. Lunt and S. Masina for useful suggestions and the Centro Euro-Mediterraneo sui Cambiamenti Climatici" (Bologna) where part of the work was carried out, and acknowledges the support of the People Programme (Marie Curie Actions) of the European Union 7th Framework Programme (FP7 2007-2013, grant agreement 29020). S.A.C. was supported by FP7 2007-2013 through the NACLIM project (grant agreement 308299),and from the MASTS pooling initiative (Marine Alliance for Science and Technology for Scotland, funded by the Scottish Funding Council, grant reference HR09011, and contributing institutions). A.T.B., A.C.C., J.J.-M.H. and N.P.H were supported by NERC's National Capability Programme. The simulation was conducted on HECToR, the UK's national high-performance computing service.

References

Antonov, J.I., Locarnini, R.A., Boyer, T.P., Mishonov, A.V., Garcia, H.E., 2006. World Ocean Atlas 2005, Volume 2: Salinity. In: Levitus, S. (Ed.), World Ocean Atlas 2005NOAA Atlas NESDIS. U.S. Government Printing Office, Washington, p. 182.

Bacon, S., 2002. The dense overflows from the Nordic Seas into the deep North Atlantic. Presented at: ICES Symposium 100 Years of Science Under ICES, Helsinki, Finland, 1–4 August 2000 215, pp. 148–155.

Bacon, S., 2010. RRS Discovery Cruise 332. Tech. Rep., National Oceanography Centre Cruise Report, Southampton, UK.

Beismann, J.O., Barnier, B., 2004. Variability of the meridional overturning circulation of the North Atlantic: sensitivity to overflows of dense water masses. Ocean Dyn. 54 (5), 92.

Belkin, I.M., Cornillon, P.C., Sherman, K., 2009. Fronts in large marine ecosystems. Prog. Oceanogr. 81, 223–236.

Biri, S., 2013. Data-Driven Batch Scheduling(Ph.D. thesis) Department of Earth Sciences, University of Hamburg.

Blaker, A.T., Hirschi, J.J.-M., McCarthy, G., Sinha, B., Taws, S., Marsh, R., Coward, A., de Cuevas, B., 2014. Historical analogues of the recent extreme minima observed in the Atlantic meridional overturning circulation at 26°N. Clim. Dyn. 1–17.

Blanke, B., Delecluse, P., 1993. Low frequency variability of the tropical Atlantic Ocean simulated by a general circulation model with mixed layer physics. J. Phys. Oceanogr. 23, 1363–1388.

Bower, A.S., von Appen, W.-J., 2008. Interannual variability in the pathways of the north Atlantic current over the mid-Atlantic ridge and the impact of topography. J. Phys. Oceanogr. 38 (1), 104–120.

Brayshaw, D.J., Hoskins, B., Blackburn, M., 2011. The basic ingredients of the North Atlantic storm track. Part II: sea surface temperatures. J. Atmos. Sci. 68 (8), 1784–1805.

Brodeau, L., Barnier, B., Treguier, A.-M., Penduff, T., Gulev, S., 2010. An ERA40-based atmospheric forcing for global ocean circulation models. Ocean Model. 31 (3–4), 88–104.

Bryden, H.L., King, B.A., McCarthy, G.D., McDonagh, E.L., 2014. Impact of a 30% reduction in Atlantic meridional overturning during 2009–2010. Ocean Sci. Discuss. 11 (2), 789–810.

Buchan, J., Hirschi, J.J.M., Blaker, A.T., Sinha, B., 2014. North Atlantic SST anomalies and the cold North European weather events of winter 2009/10 and December 2010. Mon. Weather Rev. 142 (2), 922–932.

Carton, J.A., Grodsky, S.A., Liu, H., 2008. Variability of the oceanic mixed layer, 1960–2004. J. Clim. 21 (5), 1029–1047.

Chanut, J., Barnier, B., Large, W., Debreu, L., Penduff, T., Molines, J.-M., Mathiot, P., 2008. Mesoscale eddies in the Labrador Sea and their contribution to convection and restratification. J. Phys. Oceanogr. 38, 1617–1643.

Chelton, D.B., Xie, S.-P., 2010. Coupled ocean–atmosphere interaction at oceanic mesoscales. Oceanography 23 (4), 52–69.

Cravatte, S., Madec, G., Izumo, T., Menkes, C., Bozec, A., 2007. Progress in the 3-D circulation of the eastern equatorial Pacific in a climate. Ocean Model. 28 (19), 28–48.

Cromwell, D., Challenor, P.G., New, A.L., Pingree, R.D., 1996. Persistent westward flow in the Azores Current as seen from altimetry and hydrography. J. Geophys. Res. 101, 11923–11933.

Cunningham, S.A., Kanzow, T., Rayner, D., Baringer, M.O., Johns, W.E., Marotzke, J., Longworth, H.R., Grant, E.M., Hirschi, J.J.-M., Beal, L.M., Meinen, C.S., Bryden, H.L., 2007. Temporal variability of the Atlantic meridional overturning circulation at 26.5°N. Science 317 (5840), 935–938.

Danabasoglu, G., Large, W.G., Briegleb, B.P., 2010. Climate impacts of parameterized Nordic sea overflows. J. Geophys. Res. Oceans 115 (C11).

de Boyer Montégut, C., Madec, G., Fischer, A., Lazar, A., Iudicone, D., 2004. Mixed layer depth over the global ocean: an examination of profile data and a profile-based climatology. J. Geophys. Res. Oceans 109 (C12).

Desbruyères, D., Mercier, H., Thierry, V., 2014. On the mechanisms behind decadal heat content changes in the eastern subpolar gyre. Prog. Oceanogr. http://dx.doi.org/10.1016/j.pocean.2014.02.005.

Deshayes, J., Treguier, A.-M., Barnier, B., Lecointre, A., Sommer, J.L., Molines, J.-M., Penduff, T., Bourdallé-Badie, R., Drillet, Y., Garric, G., Benshila, R., Madec, G., Biastoch, A., Bning, C.W., Scheinert, M., Coward, A.C., Hirschi, J.J.-M., 2013. Oceanic hindcast simulations at high resolution suggest that the Atlantic MOC is bistable. Geophys. Res. Lett. 40 (12), 3069–3073.

Dickson, R., Brown, J., 1994. The production of North-Atlantic deep waters — sources, rates, and pathways. J. Geophys. Res. Oceans 99 (C6), 12319–12341.

Miniconference on Observation and Modeling of North Atlantic Deep Water Formation and its Variability. Columbia University, Lamont Doherty Earth Observations, Palisades, NY (November).

Dickson, R., Rudels, B., Dye, S., Karcher, M., Meincke, J., Yashayaev, I., 2007. Current estimates of freshwater flux through Arctic and subarctic seas. Prog. Oceanogr. 73 (3–4), 210–230.

Döscher, R., Redler, R., 1997. The relative importance of northern overflow and subpolar deep convection for the North Atlantic thermohaline circulation. J. Phys. Oceanogr. 27 (9), 1894–1902.

DRAKKAR Group, 2007. Eddy-permitting ocean circulation hindcasts of past decades. Tech. rep. CLIVAR Exchanges 12.

Duchez, A., Frajka-Williams, E., Castro, N., Hirschi, J.J.-M., Coward, A., 2014. Seasonal to interannual variability in density around the Canary Islands and their influence on the Atlantic meridional overturning circulation at 26°N. J. Geophys. Res. Oceans 119 (3), 1843–1860.

Eden, C., Böning, C.W., 2002. Sources of eddy kinetic energy in the Labrador Sea. J. Phys. Oceanogr. 32, 3346–3363.

Eden, C., Willebrand, J., 2001. Mechanism of interannual to decadal variability of the North Atlantic circulation. J. Clim. 14 (10), 2266–2280.

Eldevik, T., Nilsen, J.E.O., Iovino, D., Olsson, K.A., Sando, A.B., Drange, H., 2009. Observed sources and variability of Nordic seas overflow. Nat. Geosci. 2 (6), 405–409.

Fichefet, T., Maqueda, M., 1997. Sensitivity of a global sea ice model to the treatment of ice thermodynamics and dynamics. J. Geophys. Res. Oceans 102 (C6), 12609–12646.

Fratantoni, P.S., McCartney, M.S., 2010. Freshwater export from the Labrador Current to the North Atlantic Current at the Tail of the Grand Banks of Newfoundland. Deep-Sea Res. I Oceanogr. Res. Pap. 57 (2), 258–283.

Gao, Y.-Q., Yu, L., 2008. Subpolar gyre index and the North Atlantic meridional overturning circulation in a coupled climate model. Atmos. Ocean. Sci. Lett. 1 (1), 29–32.

Garnier, V., Schopp, R., 1999. Wind influence on the mesoscale activity along the Gulf Stream and the North Atlantic currents. J. Geophys. Res. Oceans 104 (C8), 18087–18110 (1978–2012).

Gelderloos, R., Katsman, C.A., Drijfhout, S.S., 2011. Assessing the roles of three eddy types in restratifying the Labrador Sea after deep convection. J. Phys. Oceanogr. 41 (11), 2102–2119.

Grist, J.P., Josey, S.A., Bohme, L., Meredith, M.P., Davidson, F.J.M., Stenson, G.B., Hammill, M.O., 2011. Temperature signature of high latitude Atlantic boundary currents revealed by marine mammal-borne sensor and Argo data. Geophys. Res. Lett. 38.

Gulev, S., Barnier, B., Knochel, H., Molines, J., Cottet, M., 2003. Water mass transformation in the North Atlantic and its impact on the meridional circulation: insights from an ocean model forced by NCEP-NCAR reanalysis surface fluxes. J. Clim. 16 (19), 3085–3110.

Haine, T., Böning, C., Brandt, P., Fischer, J., Funk, A., Kieke, D., Kvaleberg, E., Rhein, M., Visbeck, M., 2008. North Atlantic deep water transformation in the Labrador Sea, recirculation through the subpolar gyre, and discharge to the subtropics. Defining the Role of the Northern Seas in Climate. Arctic Subarctic Ocean Fluxes. Springer, Netherlands, pp. 653–701.

Häkkinen, S., Rhines, P.B., 2004. Decline of subpolar North Atlantic circulation during the 1990s. Science 304 (5670), 555–559.

Häkkinen, S., Rhines, P.B., Worthen, D.L., 2013. Northern North Atlantic Sea surface height and ocean heat content variability. J. Geophys.Res. Oceans 118 (7), 3670–3678.

Hall, M.M., Torres, D.J., Yashayaev, I., 2013. Absolute velocity along the AR7W section in the Labrador Sea. Deep-Sea Res. I Oceanogr. Res. Pap. 72, 72–87.

Hansen, B., Østerhus, S., 2000. North Atlantic–Nordic Seas exchanges. Prog. Oceanogr. 45 (2), 109–208.

Hansen, B., Østerhus, S., 2007. Faroe Bank Channel overflow 1995–2005. Prog. Oceanogr. 75 (4), 817–856.

Hátún, H., Sandø, A.B., Drange, H., Hansen, B., Valdimarsson, H., 2005. Influence of the Atlantic subpolar gyre on the thermohaline circulation. Science 309 (5742), 1841–1844.

Higginson, S., Thompson, K.R., Huang, J., Veronneau, M., Wright, D.G., 2011. The mean surface circulation of the North Atlantic subpolar gyre: a comparison of estimates derived from new gravity and oceanographic measurements. J. Geophys. Res. Oceans 116.

Holliday, N.P., Bacon, S., Allen, J., McDonagh, E.L., 2009. Circulation and transport in the western boundary currents at Cape Farewell, Greenland. J. Phys. Oceanogr. 39 (8), 1854–1870.

Hughes, S.L., Holliday, N.P., Gaillard, F., the ICES Working Group on Oceanic Hydrography, 2012. Variability in the ICES/NAFO region between 1950 and 2009: observations from the ICES report on ocean climate. ICES J. Mar. Sci. J. Conseil 69 (5), 706–719.

Ingleby, B., Huddleston, M., 2007. Quality control of ocean temperature and salinity profiles — historical and real-time data. J. Mar. Syst. 65 (1–4), 158–175.

36th International Liege Colloquium on Ocean Dynamics, Liege, Belgium, May 03–07.

IOC, IHO and BODC, 2003. Centenary Edition of the GEBCO Digital Atlas, published on CD-ROM on behalf of the Intergovernmental Oceanographic Commission and the International Hydrographic Organization as part of the General Bathymetric Chart of the Oceans. Tech. Rep. British Oceanographic Data Centre, Liverpool.

Jochumsen, K., Quadfasel, D., Valdimarsson, H., Jonsson, S., 2012. Variability of the Denmark Strait overflow: moored time series from 1996–2011. J. Geophys. Res. 17 (C12003).

Kanzow, T., Cunningham, S.A., Johns, W.E., Hirschi, J.J.-M., Marotzke, J., Baringer, M.O., Meinen, C.S., Chidichimo, M.P., Atkinson, C., Beal, L.M., Bryden, H.L., Collins, J., 2010. Seasonal variability of the Atlantic meridional overturning circulation at 26.5°N. J. Clim. 23 (21), 5678–5698.

Käse, R.H., Krauss, W., 1996. The Gulf Stream, the North Atlantic Current, and the origin of the Azores current. The Warm watersphere of the North Atlantic Ocean. pp. 291–337.

Katsman, C., Spall, M., Pickart, R., 2004. Boundary current eddies and their role in the restratification of the Labrador Sea. J. Phys. Oceanogr. 34 (9), 1967–1983.

Lazier, J., Hendry, R., Clarke, A., Yashayaev, I., Rhines, P., 2002. Convection and restratification in the Labrador Sea, 1990–2000. Deep-Sea Res. I Oceanogr. Res. Pap. 49 (10), 1819–1835.

Lévy, C., Estublier, A., Madec, G., 2001. Choice of an advection scheme for biogeochemical models. Geophys. Res. Lett. 17 (1), 3725–3728.

Locarnini, R.A., Mishonov, A.V., Antonov, J.I., Boyer, T.P., Garcia, H.E., 2006. World Ocean Atlas 2005, Volume 1: Salinity. In: Levitus, S. (Ed.), NOAA Atlas NESDIS 61. U.S. Government Printing Office, Washington, p. 182.

Macrander, A., Send, U., Valdimarsson, H., Jonsson, S., Käse, R., 2005. Interannual changes in the overflow from the Nordic Seas into the Atlantic Ocean through Denmark Strait. Geophys. Res. Lett. 32 (6).

Madec, G., 2008. NEMO ocean engine. Note du Pole de modélisation, Institut Pierre-Simon Laplace (IPSL), France.

Madec, G., Imbard, M., 1996. A global ocean mesh to overcome the North Pole singularity. Clim. Dyn. 12 (6), 381–388.

Marsh, R., de Cuevas, B.A., Coward, A.C., Jacquin, J., Hirschi, J.J.-M., Aksenov, Y., Nurser, A.G., Josey, S.A., 2009. Recent changes in the North Atlantic circulation simulated with eddy-permitting and eddy-resolving ocean models. Ocean Model. 28 (4), 226–239.

McCarthy, G., Frajka-Williams, E., Johns, W.E., Baringer, M.O., Meinen, C.S., Bryden, H.L., Rayner, D., Duchez, A., Roberts, C., Cunningham, S.A., 2012. Observed interannual variability of the Atlantic meridional overturning circulation at 26.5°N. Geophys. Res. Lett. 39 (19).

Pacanowski, R., Gnanadesikan, A., 1998. Transient response in a z-level ocean model that resolves topography with partial cells. Mon. Weather Rev. 126 (12), 3248–3270.

Penduff, T., Barnier, B., Dewar, W.K., O'Brien, J.J., 2004. Dynamical response of the oceanic eddy field to the North Atlantic oscillation: a model-data comparison. J. Phys. Oceanogr. 34 (12), 2615–2629.

Popova, E.E., Yool, A., Coward, A.C., Aksenov, Y.K., Alderson, S.G., de Cuevas, B.A., Anderson, T.R., 2010. Control of primary production in the Arctic by nutrients and light: insights from a high resolution ocean general circulation model. Biogeosciences 7 (11), 3569–3591.

Prandle, D., Ballard, G., Flatt, D., Harrison, J.A., Jones, S.E., Knight, P.J., Loch, S., McManus, J., Player, R., Tappin, A., 1996. Combining modelling and monitoring to determine fluxes of water, dissolved and particulate metals through the Dover Strait. Cont. Shelf Res. 16, 237–257.

Quadfasel, D., Käse, R., 2007. Present-day manifestation of the Nordic Seas overflows. In: Schmittner, A., Chiang, J.C.H., Hemmings, S.R. (Eds.), Ocean Circulation: Mechanisms and ImpactsGeophysical Monograph. American Geophysical Union, Washington.

Quartly, G., de Cuevas, B., Coward, A., 2013. Mozambique Channel eddies in GCMs: a question of resolution and slippage. Ocean Model. 63, 56–67.

Rattan, S., Myers, P.G., Treguier, A.-M., Theetten, S., Biastoch, A., Böning, C.W., 2010. Towards an understanding of Labrador Sea salinity drift in eddy-permitting simulations. Ocean Model. 35 (1–2), 77–88.

Rayner, D., Hirschi, J.J.-M., Kanzow, T., Johns, W.E., Wright, P.G., Frajka-Williams, E., Bryden, H.L., Meinen, C.S., Baringer, M.O., Marotzke, J., Beal, L.M., Cunningham, S.A., 2011. Monitoring the Atlantic meridional overturning circulation. Deep-Sea Res. II Top. Stud. Oceanogr. 58 (1718), 1744–1753.

Renner, A.H.H., Heywood, K.J., Thorpe, S.E., 2009. Validation of three global ocean models in the Weddell Sea. Ocean Model. 30 (1), 1–15.

Reynolds, R.W., Smith, T.M., 1994. Improved global sea surface temperature analyses using optimum interpolation. J. Clim. 7, 929–948.

Reynolds, R.W., Rayner, N.A., Smith, T.M., Stokes, D.C., Wang, W., 2002. An improved in situ and satellite SST analysis for climate. J. Clim. 15, 1609–1625.

Rhein, M., Kieke, D., Huettl-Kabus, S., Rossler, A., Mertens, C., Meissner, R., Klein, B., Böning, C.W., Yashayaev, I., 2011. Deep water formation, the subpolar gyre, and the meridional overturning circulation in the subpolar North Atlantic. Deep-Sea Res. II Top. Stud. Oceanogr. 58 (17–18), 1819–1832.

Roach, A., Aagaard, K., Pease, C., Salo, S., Weingartner, T., Pavlov, V., Kulakov, M., 1995. Direct measurements of transport and water properties through the Bering Strait. J. Geophys. Res. Oceans 100 (C9), 18443–18457.

Robson, J., Sutton, R., Lohmann, K., Smith, D., Palmer, M., 2012a. Causes of the rapid warming of the North Atlantic Ocean in the mid 1990s. J. Clim. 25 (5), 4116–4134.

Robson, J.I., Sutton, R.T., Smith, D.M., 2012b. Initialized decadal predictions of the rapid warming of the North Atlantic Ocean in the mid 1990s. Geophys. Res. Lett. 39 (19).

Saunders, P.M., 1990. Cold outflow from the Faroe bank channel. J. Phys. Oceanogr. 20 (1), 29–43.

Smeed, D.A., McCarthy, G., Cunningham, S.A., Frajka-Williams, E., Rayner, D., Johns, W.E., Meinen, C.S., Baringer, M.O., Moat, B.I., Duchez, A., Bryden, H.L., 2013. Observed decline of the Atlantic meridional overturning circulation 2004 to 2012. Ocean Sci. Discuss. 10 (5), 1619–1645.

Smith, R.D., Maltrud, M.E., Bryan, F.O., Hecht, M.W., 2000. Numerical simulation of the North Atlantic Ocean at 1/10°. J. Phys. Oceanogr. 30, 1532–1561.

Sonnewald, M., Hirschi, J.J.-M., Marsh, R., 2013. Oceanic dominance of interannual subtropical North Atlantic heat content variability. Ocean Sci. Discuss. 10 (1), 27–53.

Stammer, D., Wunsch, C., 1999. Temporal changes in eddy energy of the oceans. Deep-Sea Res. II Top. Stud. Oceanogr. 46 (1), 77–108.

Stammer, D., Wunsch, C., Ueyoshi, K., 2006. Temporal changes in ocean eddy transports. J. Phys. Oceanogr. 36 (3), 543–550.

Stein, M., 2005. North Atlantic subpolar gyre warming — impacts on Greenland offshore waters. J. Northwest Atl. Fish. Sci. 36, 43–54.

Straneo, F., Saucier, F., 2008. The outflow from Hudson strait and its contribution to the Labrador Current. Deep-Sea Res. I 55, 926–946.

Talandier, C., Deshayes, J., Treguier, A.-M., Capet, X., Benshila, R., Debreu, L., Dussin, R., Molines, J.-M., Madec, G., 2014. Improvements of simulated Western North Atlantic current system and impacts on the AMOC. Ocean Model. 76, 1–19.

Tréguier, A.M., Theetten, S., Chassignet, E.P., Penduff, T., Smith, R., Talley, L., Beismann, J.O., Böning, C., 2005. The North Atlantic subpolar gyre in four high-resolution models. J. Phys. Oceanogr. 35 (5), 757–774.

Treguier, A.M., Deshayes, J., Lique, C., Dussin, R., Molines, J.M., 2012. Eddy contributions to the meridional transport of salt in the North Atlantic. J. Geophys. Res. Oceans 117 (C5).

Treguier, A.M., Deshayes, J., Le Sommer, J., Lique, C., Madec, G., Penduff, T., Molines, J.-M., Barnier, B., Bourdalle-Badie, R., Talandier, C., 2014. Meridional transport of salt in the global ocean from an eddy-resolving model. Ocean Sci. 10 (2), 243–255.

U.S. Department of Commerce, 2006. National Geophysical Data Center: 2-minute Gridded Global Relief Data (ETOPO2v2). Tech. rep. National Oceanic and Atmospheric Administration.

Våge, K., Pickart, R.S., Thierry, V., Reverdin, G., Lee, C.M., Petrie, B., Agnew, T.A., Wong, A., Ribergaard, M.H., 2009. Surprising return of deep convection to the subpolar North Atlantic Ocean in winter 2007–2008. Nat. Geosci. 2, 590–614.

Våge, K., Pickart, R.S., Sarafanov, A., Knutsen, Ø., Mercier, H., Lherminier, P., van Aken, H.M., Meincke, J., Quadfasel, D., Bacon, S., 2011. The Irminger gyre: circulation, convection, and interannual variability. Deep-Sea Res. I Oceanogr. Res. Pap. 58 (5), 590–614.

Voet, G., Quadfasel, D., 2010. Entrainment in the Denmark Strait overflow plume by meso-scale eddies. Ocean Sci. 6 (1), 301–310.

Willebrand, J., Barnier, B., Böning, C.W., Dieterich, C., Killworth, P.D., Le Provost, C., Jia, Y.L., Molines, J.-M., New, A.L., 2001. Circulation characteristics in three eddy-permitting models of the North Atlantic. Prog. Oceanogr. 48 (2–3), 123–161.

Woodgate, R.A., Aagaard, K., Weingartner, T., 2005. Monthly temperature, salinity and transport variability of the Bering Strait throughflow. Geophys. Res. Lett. 32 (56).

Yashayaev, I., 2007. Hydrographic changes in the Labrador Sea, 1960–2005. Prog. Oceanogr. 73 (3–4), 242–276.

Zhang, R., Delworth, T.L., Rosati, A., Anderson, W.G., Dixon, K.W., Lee, H.-C., Zeng, F., 2011. Sensitivity of the North Atlantic Ocean circulation to an abrupt change in the Nordic Sea overflow in a high resolution global coupled climate model. J. Geophys. Res. Oceans 116 (C12).